THE ROLE OF NEBULIN AND ITS C-TERMINUS IN SARCOMERIC STRUCTURE, FUNCTION, AND DISEASE

By

Frank W. Li

Copyright © Frank W. Li 2018

A Dissertation Submitted to the Faculty of the

DEPARTMENT OF CELLULAR AND MOLECULAR MEDICINE

In Partial Fulfillment of the Requirements

For the Degree of

DOCTOR OF PHILOSOPHY

In the Graduate College

THE UNIVERSITY OF ARIZONA

2018

THE UNIVERSITY OF ARIZONA
GRADUATE COLLEGE

As members of the Dissertation Committee, we certify that we have read the dissertation prepared by Frank W. Li titled The Role of Nebulin and Its C-terminus in Sarcomeric Structure, Function, and Disease and recommend that it be accepted as fulfilling the dissertation requirement for the Degree of Doctor of Philosophy.

Hendrikus L. Granzier (Chair) Date: 08/14/18

Carol C. Gregorio Date: 08/14/18

Thomas C. Doetschman Date: 08/14/18

Samantha Harris Date: 08/14/18

Final approval and acceptance of this dissertation is contingent upon the candidate's submission of the final copies of the dissertation to the Graduate College.

I hereby certify that I have read this dissertation prepared under my direction and recommend that it be accepted as fulfilling the dissertation requirement.

Dissertation Director: Hendrikus L. Granzier Date: 08/14/18

2

STATEMENT BY THE AUTHOR

This dissertation has been submitted in partial fulfillment of the requirements for an advanced degree at the University of Arizona and is deposited in the University Library to be made available to borrowers under rules of the Library.

Brief quotations from this dissertation are allowable without special permission, provided that an accurate acknowledgement of the source is made. Requests for permission for extended quotation from or reproduction of this manuscript in whole or in part may be granted by the head of the major department or the Dean of the Graduate College when in his or her judgment the proposed use of the material is in the interests of scholarship. In all other instances, however, permission must be obtained from the author.

SIGNED: Frank W. Li

Acknowledgements

I would like to thank my mentor, Dr. Henk Granzier, for helping me become a better scientist. I came into this field not knowing what I wanted to do with my life and found a passion in research and the intricacies of muscle. Thank you for allowing me the chance to learn and grow in your lab. I hope that what I have learned under your tutelage helps me become an active and prominent member of the field of muscle biology.

To the past and present members of the Granzier lab, thank you all for making my time as a PhD some of the best years of my life. Whether it was in the lab or at various social events, I always enjoyed the interactions. I learned a great deal, both as a scientist and as a person, and came out better for it. I was richer for having known you all.

Many thanks to my committee members: Dr. Carol Gregorio, Dr. Tom Doetschman, Dr. Sam Harris, and Dr. Coen Ottenheijm. Your comments and insights helped me organize my project and complete my research in a timely fashion.

Thanks to my funding at the National Institute of Arthritis, Musculoskeletal, and Skin Diseases.

As Mei Methawasin would remind us, thank you to all the animals that have contributed to my project.

Finally, a special thank you must go out to my family. To my mom and dad, thank you for supporting my decision to stay in research, even if what I do still eludes you to this day. And thanks to my sister who kept me sane and connected to the rest of the family through these many years.

Contents

List of Figures and Tables

Abstract

Nebulin is a large skeletal muscle protein wound around the thin filaments, with its C-terminus embedded within the Z-disk and its N-terminus extending out towards the thin filament pointed end. Studies into nebulin's function have been limited by the conventional knockout model's fragility and nebulin's role in adult muscle remains poorly understood. Therefore, a nebulin knockout model that survives into adulthood is needed. Additionally, a domain-specific study of nebulin's C-terminus would allow for a better understanding of changes at the Z-disk and how that could contribute to nemaline myopathy. This dissertation examines two novel models in order to address these points. Characterization of a conditional nebulin knockout model (Neb cKO), which delayed nebulin deletion using a MCK-Cre transgene, found severe myopathy and a persistent force deficit. Changes in MHC isoform elucidated the biological causes of these deficits. The nebulin truncation model removed the final two unique C-terminal domains, the serine-rich region and the SH3 domain ($Neb^{\Delta 163\text{-}165}$). Homozygous $Neb^{\Delta 163\text{-}165}$ mice that survive past the neonatal stage exhibit a mild weight deficit. Characterization of these mice revealed that the truncation caused a moderate myopathy phenotype reminiscent of nemaline myopathy despite the majority of nebulin being localized properly in the thin filaments. This phenotype included muscle weight loss, changes in sarcomere structure, as well as a decrease in force production. GST pulldown experiments found novel binding partners with the serine-rich region, several of which are associated with myopathies. The comparison of these two models emphasizes the role of nebulin's C-terminus in the muscle sarcomere, finding that this small region is necessary for proper sarcomeric development and shows that its loss is sufficient to induce myopathy.

Chapter 1: Introduction

The Skeletal Muscle Sarcomere

The sarcomere is the most basic functional unit of muscle. These units are arranged linearly within myofibrils, which bundle up to form muscle fibers. These fibers are connected via a dense network of connective tissues, collectively forming much larger muscle fascicles which are connected at the ends to bone via tendons. While the force produced by a single sarcomere is inherently small, the cooperation of thousands of sarcomeres working in unison is what ultimately allows for whole muscle contraction and movement. This means that the key component contributing to muscle contraction is the proper formation and function of the individual sarcomere.

A sarcomere is comprised of three major filaments (Figure 1). First is the thick filament, which contains the molecular motor myosin and acts as the primary force generating protein within the sarcomere. This creates a well-defined region of bundled myosin proteins known as the A-band. Next is the thin filament, which is shaped by the presence of filamentous actin and serves as a track for myosin to move along. During contraction, myosin heads grab onto the actin thin filaments and pull, shortening the sarcomere and generating strength (Huxley & Hanson, 1954). This motion then causes the thin filaments to slide past the thick filaments in what is now commonly known as the Sliding Filament Theory. The region occupied by thin filaments only is termed the I-band and due to this sliding motion, can shrink during contraction. These two filaments, along with accessory proteins that respond to the ATP and calcium concentrations within a cell allow the sarcomere to generate active tension. The third major filament of the muscle sarcomere is titin, which contrary to the other two filaments acts more as a spring and generates passive tension within the sarcomere (Siegfried Labeit & Kolmerer, 1995b).

Figure 1: Overview of the Muscle Sarcomere

The muscle sarcomere is comprised of three primary filaments: actin thin filaments, myosin thick filaments, and titin. Actin and myosin act in conjunction to provide active tension to the whole muscle while titin provides passive tension. Accessory proteins along the thin and thick filament regulate contractile function while phosphorylation of titin adjusts passive tension. One major player in thin filament length regulation is nebulin, which winds around the thin filaments.

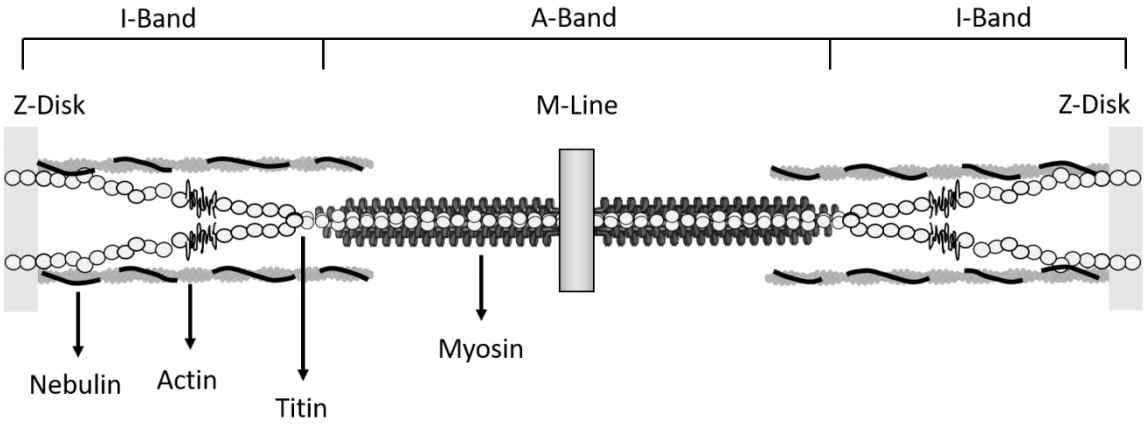

These major filaments have attachment points at the M-band, the Z-disk, or in the case of titin, both (Siegfried Labeit & Kolmerer, 1995b). The Z-disk is a network of various structural proteins such as α-actinin, filamin c, and myotilin existing in the middle of the I-band. This dense structure serves as an attachment point for titin's N-terminus as well as the barbed end of the actin thin filaments. In the middle of the sarcomere is the aptly named M-band, which is a structure comprised of a network of myomesin and obscurin proteins (Grove et al., 1984; Young, Ehler, & Gautel, 2001). These two proteins connect each individual thick filament to its neighbors in a three-dimensional space, providing lateral tension to the sarcomere and stability to the A-band. The presence of both these attachment zones is necessary when creating such an ordered structure as skeletal muscles.

The thin and thick filaments within the sarcomere both have a highly defined length resulting in the sarcomere, and consequently the muscle, having a semi-crystalline structure (Elliott, 1979; Huxley & Hanson, 1954). Alterations to this structure can often result in an inefficient, or even non-functional, sarcomere. One common cause of dysfunctional sarcomeres is changes within the actin thin filament. This filament needs to be at a defined length for the myosin heads to contract in unison and pull with even force across the entirety of the muscle. Because of this requirement, there are several proteins that facilitate thin filament length regulation. And when looking at contractile dysfunction, one must begin at the development of the sarcomere, which inevitably requires an understanding of the protein nebulin.

Nebulin: The Large Multifunctional Protein

Nebulin is a large filamentous protein that is found wrapped around almost the entirety of the actin thin filament. Its C-terminus is embedded within the Z-disks and its N-terminus

extends out towards the pointed ends of the thin filaments (Figure 2). This makes it one of largest proteins found in the body, existing anywhere between 600 and 800 kDa. It is translated almost exclusively in skeletal muscle and is thought to act as a backbone or guide for actin during development (S. Labeit et al., 1991). This hypothesis originally arose from the observation that nebulin's size had a positive correlation with the predicted thin filament lengths in different species (Kruger, Wright, & Wang, 1991; S. Labeit et al., 1991). The study of the structure of nebulin revealed it was comprised primarily of homologous 35-amino acid modules that each contained an actin-binding motif (Siegfried Labeit & Kolmerer, 1995a), strengthening the hypothesis that nebulin regulated thin filament lengths. These motifs were spaced at a distance that aligned with the periodicity of actin monomers within the thin filament. These modules were organized into 25 homologous, 7-module super repeats that each contained tropomyosin binding sites, further supporting the hypothesis that this protein would integrate tightly to the thin filaments.

The remaining 3% of the protein comprised of a glutamic acid-rich region at the N-terminus and both a serine-rich region and a SH3 domain at the C-terminus. And while the individually unique domains at the N- and C-terminus were noted, it was initially proposed that the actin-binding modules that formed 97% of the protein defined nebulin's primary function as a thin filament length regulator. Following the publication of nebulin's sequence, studies also found that the first three actin-binding modules at the N-terminus of nebulin, located at the pointed ends of the thin filament, could interact with tropomodulin, another accessory protein that participates instead in the maintenance of actin thin filament lengths.

Figure 2: Basic Structure of Nebulin

Nebulin is comprised primarily of actin-binding modules (M1-M206). These modules allow for nebulin to wrap around the thin filaments, spanning nearly the entirety of the structure. Its N-terminus is located near the pointed ends of the thin filaments while the C-terminus is firmly embedded within the Z-disk. Unique domains at both ends facilitate additional interactions with sarcomeric proteins.

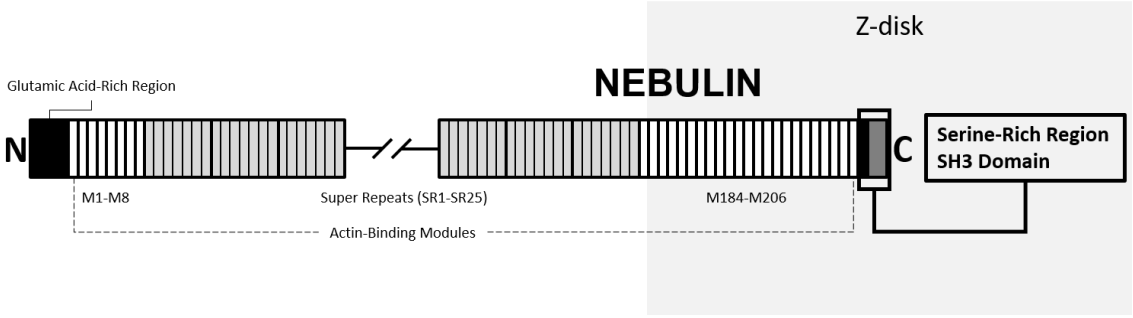

Knockout Animal Models

Studies using *in vivo* techniques saw the most rapid progression in the understanding of how nebulin is necessary for the structural and functional integrity of the muscle sarcomere. Using transgenic mouse models, two separate groups knocked out nebulin in the embryonic stage, preventing nebulin from being translated at all (Bang et al., 2006; Witt et al., 2006). Both models found that a lack of nebulin resulted in severe muscle weakness and developmental defects that prevented the mouse from living past two weeks of age. Electron microscopy revealed severe disorganization of myofibrils as well as prominent protein aggregates in line with the Z-disks. These phenotypes were highly reminiscent of a disease called nemaline myopathy (discussed below) supporting the idea that nebulin was necessary for muscle function.

Further investigation using these preliminary knockout models also found changes in other regulatory proteins within the sarcomere. For instance sarcolipin, a SERCA-inhibitor and regulator of calcium flux necessary for muscle contraction, was upregulated, resulting in slower calcium cycling (Ottenheijm et al., 2008). This resulted in the proposal of a contractile function for nebulin. The structural protein desmin was also found to be dysregulated in these diseased sarcomeres, contributing to the misalignment observed in longitudinal sections of skeletal muscle (Tonino et al., 2010). As these additional functions were proposed for nebulin, it became quickly apparent that nebulin was a protein that, if lost, would have widespread effects on the entirety of the sarcomere, from mechanical to metabolic functions. However, conventional knockout mice prevented further study of this protein in adult tissues. And as the understanding of nebulin's function increased, it became more necessary to study this large protein piece by piece to understand how individual domains of nebulin contribute to its overall function.

Nebulin's Role in Nemaline Myopathy

Concurrently, new discoveries were also being made with regards to nemaline myopathy, a largely non-progressive myopathy. Originally identified in the 1960s, this muscle disease found muscle weakness of varying severities in patients and was named after the thread-like protein aggregates found within muscle biopsies called nemaline rods (Shy, Engel, Somers, & Wanko, 1963). This disease was found to result from a recessive inheritance with an incidence of about 1 in 50,000 (North & Ryan, 2002; Wallgren-Pettersson et al., 1990). Over the next twenty-five years several genes were identified as causing nemaline myopathy: ACTA1 (Nowak et al., 1999), NEB (Pelin et al., 1999), TPM2 (Donner et al., 2002), TPM3 (Laing et al., 1995), TNNT1 (Johnston et al., 2000), CFL2 (Agrawal et al., 2007), KBTBD13 (Sambuughin et al., 2010), KLHL40 (Ravenscroft et al., 2013), KLHL41 (Gupta et al., 2013), and LMOD3 (Yuen et al., 2015). Unfortunately, a consistent problem with these patient-driven mutation studies was the lack of a genotype-phenotype correlation.

When nebulin was identified and sequenced, clinical research groups began to investigate its presence in patients with varying levels of nemaline myopathy. They predicted that this large protein was responsible for about half of all documented cases of nemaline myopathy (North & Ryan, 2002; Pelin et al., 1999). To complicate the disease, some patients were seen to produce full length nebulin while others had only small truncations at the C-terminus (Lehtokari et al., 2014; Pelin et al., 1999) (Table 1). In the efforts to catalogue patient mutations and phenotypes, researchers found that over 55% of patients with nebulin-induced nemaline myopathy (NEM2) had either frameshift or nonsense mutations that could prematurely truncate the protein (Lehtokari et al., 2014). While some of these truncations could result in a loss of nebulin through nonsense-mediated decay, the database of patient mutations suggested that a truncated, but present, nebulin could cause as severe a phenotype as a complete loss of

Table 1: C-terminal Mutations in Nemaline Myopathy Patients

Through a study of 212 pathogenic NEB variants, 83% of mutations were found to be compound heterozygous in nature. 55% of mutations studied are frameshift or nonsense mutations which may lead to protein truncation. Human nebulin contains 183 exons. Table adapted from published data (Lehtokari et al., 2014).

Nebulin Exon	**Mutation**	**Inheritance**	**Disease Classification**
Ex180	Deletion	Homozygous	Severe
Ex180	Deletion	Compound Heterozygous	Severe
Ex180	Point Mutation	Compound Heterozygous	Intermediate
Ex180	Point Mutation	Compound Heterozygous	Unspecified
Ex181	Point Mutation	Homozygous	Typical
Ex182	Point Mutation	Compound Heterozygous	Typical
Ex182	Deletion	Compound Heterozygous	Typical

the protein. Coupled with the protein aggregates frequently observed in line with the Z-disks, the idea was formed that nebulin's C-terminus could play a much larger role than previously expected.

Nebulin's C-terminus and Its Role in Muscle Hypertrophy

Attention to nebulin's C-terminus was further increased through a novel mechanism for muscle hypertrophy (Takano et al., 2010). In 2010, Takano et al. published a study suggesting that nebulin might play a role in this process. The initial observation of this study revolved around the discovery of the Neural Wiskott-Aldrich Syndrome Protein, or N-WASP, within the Z-disks of skeletal muscle. N-WASP was previously known to be utilized in branched actin filament formation. After activating the Arp2/3 complex, N-WASP would then use the Arp2/3 complex as a nucleation point and facilitate the formation of a new actin filament that branched off another filament at a 70° angle (Suetsugu, Miki, Yamaguchi, Obinata, & Takenawa, 2001). Thus, the discovery of this protein within a system comprised of linear actin filaments was interesting and warranted further investigation. Through GST pulldown, the group found that N-WASP could interact with nebulin, specifically nebulin's C-terminus. And through a coimmunoprecipitation study involving these two proteins and members of the IGF-1 growth pathway, it was clear that IGF-1 stimulation would cause the two proteins to interact. Using immunofluorescence, the group showed that following IGF-1 signaling, N-WASP would localize to the Z-disk of the sarcomere within two hours before dispersing. This correlated with a simultaneous recruitment of free actin to the thin filaments, causing the group to conclude that N-WASP was facilitating the formation of new actin filaments after IGF-1 stimulation.

Further studying nebulin's C-terminus, they determined several key points. First, N-WASP's proline-rich region was necessary for an interaction between the two proteins. Through existing research, they predicted that this was due to a commonly observed affinity between proline-rich regions and SH3 domains in other regulatory proteins (Ren, Mayer, Cicchetti, & Baltimore, 1993). Secondly this interaction was only possible as a downstream effect in response to IGF-1 growth signaling, wherein GSK-3β undergoes inhibitory phosphorylation by protein kinase B (Akt), preventing it from phosphorylating nebulin at the serine-rich region (Figure 3). Phosphomimetics of two highly conserved serines within the serine-rich region showed this nebulin-N-WASP interaction did not occur when phosphorylation was present. Finally, cross-sectional hypertrophy observed after IGF-1 treatment was attenuated when N-WASP was inhibited via siRNA. This paper concluded that nebulin's C-terminus was playing a role in muscle hypertrophy in the form of myofibrillogenesis.

SH3 Deletion Model

Following this publication, one group attempted to test this mechanism using a mouse model in which nebulin's SH3 domain had been deleted (Yamamoto et al., 2013). However, upon using the same starvation and IGF-1 injection protocol, they were unable to replicate the hypertrophy results. In fact, they were unable to confirm if N-WASP localized to the Z-disks following IGF-1 injection. While this study put the mechanism into question, it also did not address the contributions of the serine-rich region, which was implicated to be important for signaling.

Figure 3: IGF-1-Mediated Myofibrillar Hypertrophy

Hypertrophy mechanism adapted from Takano et al., 2010. Their proposed mechanism involves exogenous stimulation by IGF-1, which leads to the activation of phosphoinositide 3-kinase (PI3K), which activates protein kinase B (Akt). This inhibits glycogen synthase kinase 3 beta (GSK-3β), preventing it from phosphorylating two conserved serines in the serine-rich region (SRR) of nebulin. This allows for the interaction of the SH3 domain with the proline-rich domain (PRD) of N-WASP, activating the protein and allowing it to recruit monomeric actin.

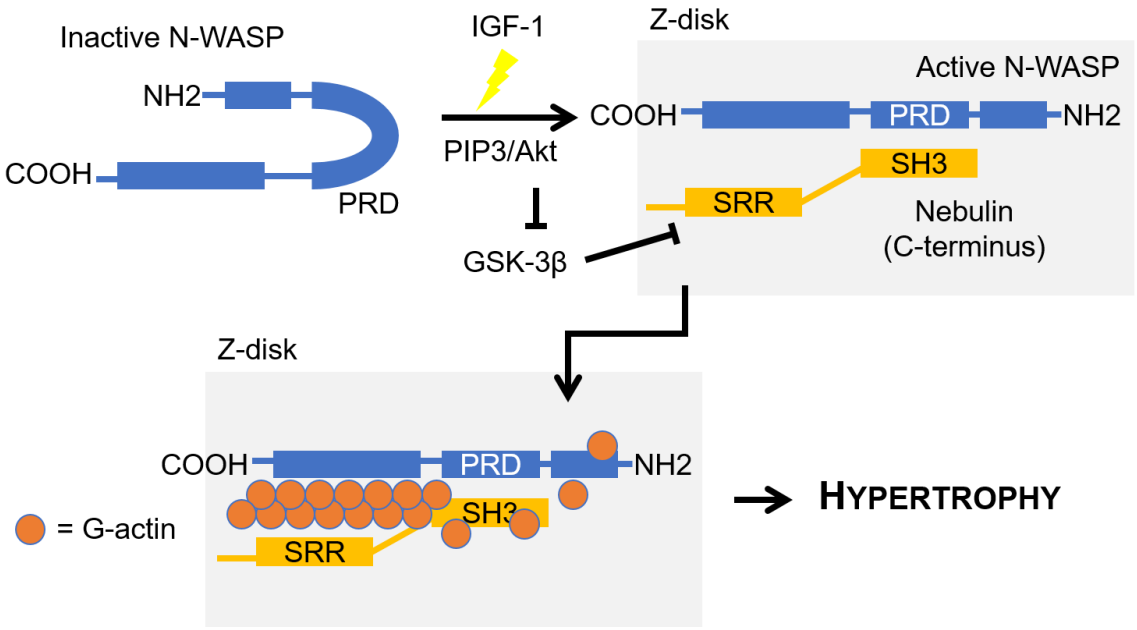

Hypothesis and Research Design

The goal of this project was to first identify nebulin's contribution to adult muscle. Here, the hypothesis was that nebulin played a role in the development of myopathy in adult muscle. However, due to the complete postnatal lethality of the conventional knockout model by two weeks (Bang et al., 2006; Witt et al., 2006), studies were unable to capture this aspect. In order to understand nebulin's role in developed muscle, a mouse model that delayed the Cre-lox-mediated knockout of nebulin using a muscle creatine kinase (MCK) promoter was created, allowing for nebulin to contribute to embryonic development. Once this first study was completed, experiments moved towards investigating how nebulin's C-terminus contributes to the development of disease.

The second portion of this project focused on the contributions of nebulin's C-terminus to the overall structure and function of the skeletal muscle sarcomere. Through observations of knockout models and patient studies, it was hypothesized that nebulin's C-terminus would be sufficient to induce myopathy. Additionally, based on the observations made by Takano et al (2010), a mouse model lacking the C-terminal domains of nebulin would result in an inability to respond to IGF-1 induced hypertrophy. To perform these studies, a second mouse model lacking specifically the two unique domains of nebulin's C-terminus, the serine-rich region and the SH3 domain, was used.

Aim 1: To study nebulin loss in mature skeletal muscle.

Hypothesis: Nebulin contributes to sarcomeric structure even in adult muscle, its loss leading to myopathy.

Nebulin's start codon was floxed and mice containing this insertion were combined with those from an MCK-Cre mouse line in order to conditionally remove nebulin from the muscle sarcomeres upon activation of the MCK promoter (Neb cKO). Muscle weights

and protein expression were studied at multiple time points. Additionally, MHC composition was studied and force development was quantified.

Aim 2: To characterize a mouse that expresses a truncated nebulin.

Hypothesis: Loss of nebulin's C-terminal domains is sufficient to cause myopathic phenotypes.

Basic characterization was performed on a mouse model lacking specifically nebulin's two C-terminal domains. Standard muscle dissections were performed to obtain whole muscle weights while whole muscle mechanics was used to quantify force production. Additionally, muscle samples were subjected to a wide array of quantification techniques including western blot, immunofluorescence, and electron microscopy.

Aim 3: To investigate protein-protein interactions with nebulin's C-terminus.

Hypothesis: Truncation of nebulin will result in a loss of interactions, some of which may contribute to phenotypes observed in the mouse model.

GST-tagged protein constructs were created to express individual domains of the C-terminus as well as the two domains in tandem. Following pulldown with whole muscle lysate, supernatants were separated via acrylamide gel. Prominent bands were analyzed via mass spectrometry and top hits were studied via western blot.

Aim 4: To assess the hypertrophic response in muscles lacking nebulin's C-terminus.

Hypothesis: Stimulation by IGF-1 and other growth stimuli that proceeds through this pathway would result in a stunted hypertrophy response.

Mice were injected intramuscularly with an IGF-1 AAV in order to mimic the IGF-1 stimulation proposed in an earlier finding (Takano et al., 2010). Mice were incubated with

this AAV for one month, establishing a long-term overexpression. Following the treatment, muscles were dissected, weighed, and embedded for CSA analysis.

Chapter 2: Methods

Generation of the Neb cKO Mouse Model

A conditional mouse model was made in which the translational start codon of the *Neb* gene was floxed and its deletion directed by a *MCK-Cre* transgene. With the help of the GEMM Core at the University of Arizona, a targeting vector containing a 2.7kb left arm of homology and a 3.0kb right arm of homology flanking exons 2 and 3 of nebulin, which contains a part of the 5'UTR and start codon for nebulin. LoxP sites were inserted in exons 2 and 3 to facilitate the gene deletion while a neomycin (*frt-neo-frt*) cassette allowed for selection of cells containing the desired mutations (Figure 4). The vector was transfected into 129/SvJ-derived embryonic stem cells and neomycin resistant cells were implanted into C57BL/6J mice. Chimeric lines were expanded and heterozygous mice were then bred to a separate C57BL/6J mouse line containing a FLPase deleter to remove the neomycin cassette. Primers P1, P2, P3, and P4 are used for genotyping. WT product from primers P1 and P3 was 122bp, floxed allele product from primers P1 and P2 was 377bp, *neo*-removed cKO allele product from primers P3 and P4 was 184bp. The primer sequences are summarized below:

P1: 5'-TCTTGACTGAGAACTAAGACTACAGC-3'

P2: 5'-CTGAAACACGGAAGGAGACAATACC-3'

P3: 5'-GATTACAACAATGTGACACTAACAGG-3'

P4: 5'-TTTTTCTTTCTTATTTTTCAGGTTTGA-3'

Figure 4: Generation of the cNeb Model

Diagram depicting the creation of a floxed allele. Targeting vector contains a neomycin cassette for resistance-based cell selection. Through the use of a MCK-Cre mouse model, the 5'UTR and start codon of nebulin was selectively removed from striated muscles. P1-4 indicate the primers used in genotyping. Diagram used with permission from (Li et al., 2015).

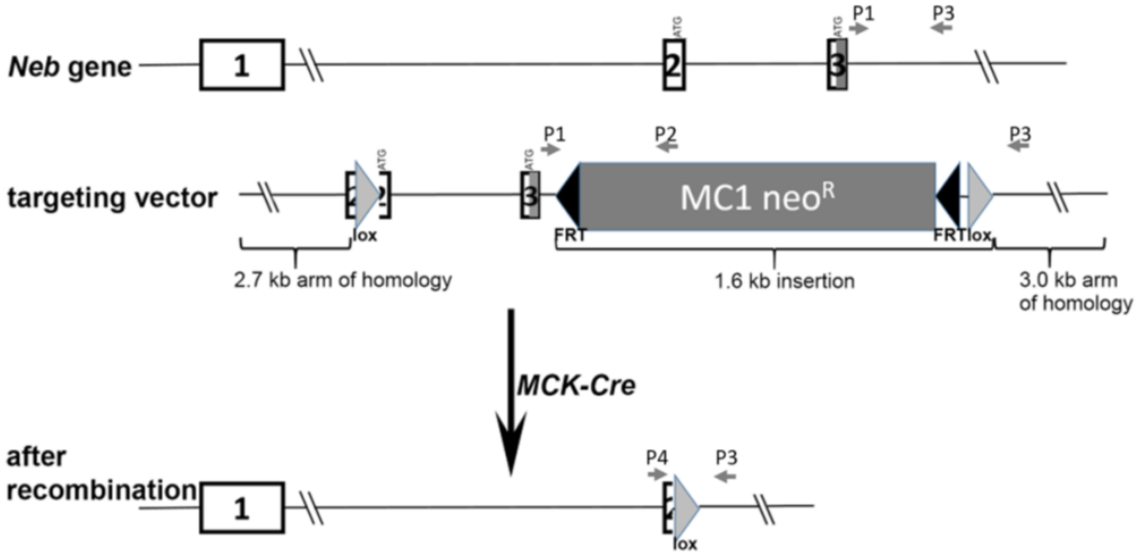

Generation of the Neb$^{\Delta 163\text{-}165}$ Mouse Model

To create this model, the final actin-binding domain, M185, based on the previously published full murine sequence was referenced (Kazmierski et al., 2003). Murine exon 163 contains the final three amino acids of M185 along with approximately half of the serine-rich region. A targeting vector containing a 3.1kb left arm of homology, a 1.8kb right arm of homology, and stop codons followed by a *frt-neo-frt* cassette was generated (Figure 5). The vector was transfected into 129/SvJ-derived embryonic stem cells and neomycin resistant cells were implanted into C57BL/6J mice. Chimeras were bred with C57BL/6J mice and *neo*-containing mice were identified via PCR using C-terminus specific primers, [forward (WT_F): 5'-CACACTAGAGGAATTATAGGTCAGC-3', neo_reverse (Neo_R): 5'-CTGGCACTCTGTCGATACCC-3']. Heterozygous mice were then bred to a separate C57BL/6J mouse line containing a FLPase deleter to remove the neomycin cassette. Mice containing the nebulin truncation but lacking the neomycin cassette was genotyped using the same forward primer and a reverse primer to the sequence downstream from the stop codons [wt_reverse (WT_R): 5'-CCGTCACTGTATGTGGAAAGG-3']. Mice were initially backcrossed to three generations before experiments were run and later backcrossed to generation 10 for verification purposes.

Figure 5: Generation of the Neb$^{\Delta 163\text{-}165}$ Model

Schematic representing homologous recombination of a generated targeting vector with the endogenous locus. Upon recombination of the STOP codons into the allele, the neomycin cassette was removed using a FLPase deleter line and the resulting truncated allele was backcrossed.

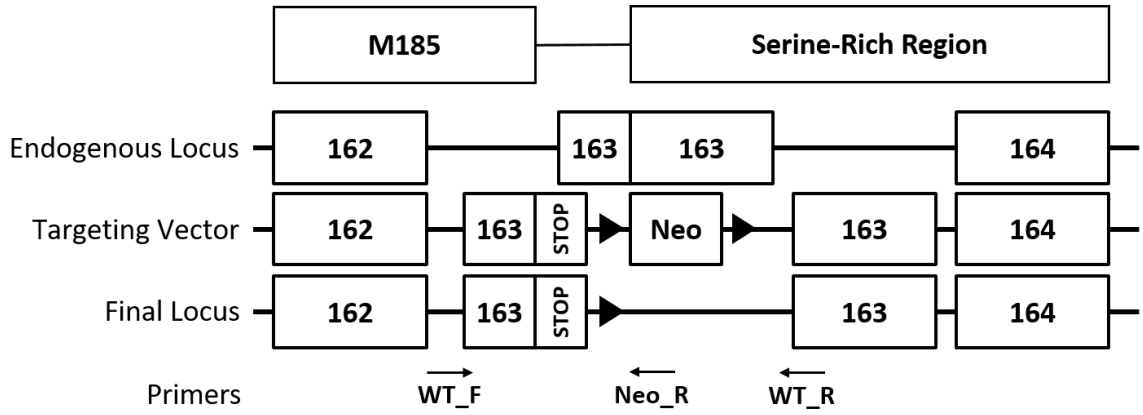

Tissue Collection

Mice were sacrificed according to approved protocols. Following the weighing of the mice, they were anesthetized via isoflurane. A toe pinch was performed to ensure complete anesthesia before cervical dislocation was performed. Hind limb muscles were then dissected and immediately flash frozen in liquid nitrogen. Following freezing, tissues were stored at -80°C. Tissue weights were normalized to tibia lengths, which were measured by electronic caliper. For each mouse, muscles from both sides were taken and weights were averaged between the two limbs. The same calculation was performed for tibia lengths before a muscle weight to tibia length normalization was performed.

Sample Preparation and Gel Electrophoresis

Muscle samples were prepared following a well-documented protocol (Warren, Krzesinski, & Greaser, 2003). Tissues were pulverized into a powder via glass Dounce tissue homogenizers pre-chilled in liquid nitrogen. Tissue powder was allowed to equilibrate in a -20°C refrigerator for twenty minutes before 50% glycerol and a urea buffer were added in a 1:40:40, sample(mg):glycerol(µL):urea(µL), ratio. Glycerol solution was made using H_2O, glycerol, and a mix of inhibitors [(in mM) 0.04 E-64, 0.16 leupeptin, 0.5 PMSF]. Urea buffer contained 8M urea, 2M thiourea, 50mM tris-HCl, 75mM dithiothreitol, 3% SDS w/v, and 0.03% bromophenol blue, with a pH of 6.8. The solution was mixed and incubated at 60°C for 10 minutes before being aliquoted and flash frozen in liquid nitrogen.

Myosin heavy chain gels were performed on 8% acrylamide gels as previously described, run for 24h at 275V before being stained with Coomassie blue (Talmadge &

Roy, 1993). Gels for the protein pulldown used 8% SDS-PAGE followed by staining with Coomassie blue. Western blots for nebulin were run with 0.8% agarose gels run for 15mA/gel for 2h 50m before being transferred to a PVDF membrane using a semi-dry transfer unit (Bio-Rad, Hercules, CA, USA). Blots for myotilin, KLHL41, and α-actinin were run using 10% SDS-PAGE before being transferred to a PVDF membrane. All blots were initially stained with Ponceau S for protein visualization. Membranes were then blocked and incubated overnight at 4°C with the appropriate primary antibodies. Both the nebulin N-terminal antibody and the SH3 antibody were provided by Dr. Siegfried Labeit (Neb-N 1:1000 rabbit, SH3 1:200 rabbit). The SRR antibody was created in a chicken host against the peptide TTQLPQQR (GenScript, NJ, USA). Other antibodies include myotilin (1:1000 rabbit ab68915, Abcam), KLHL41 (1:400 rabbit ab66605, Abcam), AIFM1 (1:1000 rabbit D39D2, Cell Signaling), and α-actinin (1:2000 mouse A7811, Sigma). Western blot for nebulin domains were normalized with MHC visualized through Ponceau S. Blots run for myotilin, KLHL41, and α-actinin were normalized to GAPDH (1:2000 mouse #GA1R, Thermo Fisher). Secondary antibodies used were conjugated with infrared fluorophores for detection (1:20000 goat anti-rabbit CF680, Biotium and 1:20000 goat anti-mouse CF790, Biotium). Infrared western blot was analyzed using an Odyssey CLx Imaging System (Li-Cor Biosciences, NE, USA). MHC viewed through Ponceau S was quantified via One-D scan EX (Scanalytics Inc., Rockville, MD, USA).

Fiber Type Identification and CSA Measurements

EDL muscles were pinned at slack length on cork and covered with OCT (Tissue-Tek). The samples were then frozen in a slurry of liquid nitrogen-cooled isopentane before being stored at -80°C. To prepare samples for cross-sections, muscles were cut mid-belly and reoriented in a cryomold containing pre-chilled OCT. 10 micron sections were

collected on glass slides and stored at -20°C for no longer than two days (Microm HM550, Thermo Fisher). Slides were equilibrated at room temperature for 10 minutes while individual samples were demarcated with a hydrophobic barrier (Vector Laboratories, Burlingame, CA, USA). Then, samples were skinned using 0.2% triton X-100 for 20 minutes followed by a 1 hour incubation with a blocking solution (2% BSA, 1% normal donkey serum) in PBS at 4°C. Primary antibodies were then applied to the sections for an overnight incubation at 4°C: laminin (1:400 rabbit L9393, Sigma-Aldrich); MHCI (1:75 IgG2b BA-F8, DSHB); MHCIIA (1:500 IgG1 SC-71, DSHB); MHCIIX exclusion (1:100 IgG1 BF-35, DSHB); MHCIIB (1:50 IgM BF-F3, DSHB). Following primary antibody incubation, sections were washed with PBS twice for 30 minutes. The matching secondary antibodies were then applied for 3-4 hours at room temperature: polyclonal Alexa Fluor 488-conjugated goat anti-rabbit [1:500 IgG (H+L) A11008, Thermo Fisher], polyclonal Alexa Fluor 350-conjugated goat anti-mouse [1:500 IgG2b A211440, Thermo Fisher], polyclonal Alexa Fluor 350-conjugated goat anti-mouse [1:500 IgG1 A21120, Thermo Fisher], and polyclonal Alexa Fluor 594-conjugated goat anti-mouse [1:500 IgM (Heavy Chain) A21044, Thermo Fisher]. Post-secondary washes included two 30 minutes washes with PBS followed by two quick rinses with water. Images were collected using an AxioCam MRc (Carl Zeiss). CSAs were quantified using the semi-automatic muscle analysis using segmentation of histology (SMASH) MATLAB application (Smith & Barton, 2014).

RNA Isolation and qRT-PCR

Tissue samples were dissected and immediately stored in RNAlater (Invitrogen). Samples were then processed using the RNeasy Fibrous Tissue Mini Kit (Qiagen). After processing, mRNA was converted to cDNA via Superscript III (Invitrogen) and diluted to

5 ng/µL for qRT-PCR. Samples were run in triplicate using TATA-binding protein (TBP) as a housekeeping gene (TBP_qF: 5'-TGCACAGGAGCCAAGAGTGAA-3', TBP_qR: 5'-CACATCACAGCTCCCCACCA-3'). Primers for nebulin were designed for Exon 40 (Neb_qF: 5'-CAAGGGTTACGACTTGAGACC-3', Neb_qR: 5'-GAAAGCCAATTTGCTTGCCTC-3'). Amplification was detected using SYBR Green and run using a Rotor-Gene Q real-time PCR cycler (Qiagen). Delta-delta Ct calculations were performed with a fluorescence threshold value of 0.1.

Immunofluorescence and Electron Microscopy

Limb muscle were dissected and immediately placed in relaxing solution (in mM: 40 BES, 10 EGTA, 6.56 $MgCl_2$, 5.88 Na-ATP, 46.35 K-propionate, 15 creatine phosphate at pH 7.0) with 1% triton X-100. At all steps, protease inhibitors were added just prior to use and samples were placed on a 2D rocker overnight at 4°C. Following skinning, muscles were washed with relaxing solution alone to remove excess triton X-100. Then, samples were placed in 50% glycerol/relaxing solution first overnight, then stored at -20°C. To obtain fiber bundles, skinned muscles were placed in sylgard dishes containing additional 50% glycerol/relaxing solution with protease inhibitors and then bundles were carefully dissected from the muscle. Bundles were held at both ends with aluminum T-clips and pinned at ~30% past slack length.

For immunofluorescence, bundles were fixed overnight at 4°C in a 10% formalin (4% formaldehyde) solution. Post-fixation, bundles were washed with PBS before being removed from the T-clips and embedded in OCT. Longitudinal sections were taken at 6µm and collected onto glass slides. These sections were fixed again in triton x-100 and blocked with normal donkey serum as described above. Primary antibodies to nebulin's N-terminus (1:300), M176-181 (1:100 rabbit, Siegfried Labeit), phalloidin 488 (1:2000

A12379, Invitrogen), and α-actinin were then applied for an overnight incubation at 4°C. Fluorescent secondary antibodies were applied after post-primary washes: polyclonal Alexa Fluor 594-conjugated goat anti-rabbit [1:600 IgG (H+L) A11012, Thermo Fisher] and polyclonal Alexa Fluor-350-conjugated goat anti-mouse [1:200 IgG (H+L) A21049, Thermo Fisher]. Deconvolution microscopy was performed using a Deltavision RT deconvolution microscope (Applied Precision) with an inverted microscope (IX70, Olympus) and the softWoRx program.

For electron microscopy, fiber bundles were briefly fixed in a 3% paraformaldehyde solution [3% PF, 2% glutaraldehyde, 0.03% tannic acid in PBS (0.01M, pH 7.2)] for 45 minutes at 4°C. Then, fixative was washed off with PBS and replaced with a 1% w/v OsO_4 solution in PBS. After this, fixed samples were gradually dehydrated in a series of ethanol washes, starting at 70% ethanol and ending with a mix of pure ethanol and propylene oxide. Then samples were infiltrated with resin (araldite/embed813) and then finally embedded in BEEM capsules (Ted Pella) for sectioning. Sections were taken at 60µm with a diamond knife set parallel to the fiber orientation. These sections were then incubated with 1% potassium permanganate followed by 0.25% lead citrate for contrast. Images were taken with transmission electron microscopy (FEI/Phillips CM12). Sarcomere density profiles were obtained via FIJI (ImageJ) and plot profiles were processed using the Fityk software.

Intact Muscle Mechanics

Whole muscle mechanics were done using an Aurora Scientific 1200A isolated muscle system (Siegfried Labeit et al., 2010; Ottenheijm, Hidalgo, Rost, Gotthardt, & Granzier, 2009). Briefly, the soleus or EDL were carefully extracted, keeping proximal and distal tendons intact. Silk suture loops (4-0 diameter) were tied to each tendon and the muscle

was attached to both a servomotor-force transducer and a stationary hook. Muscles were submerged in an oxygenated Krebs-Ringer bicarbonate solution at 30°C (in mM: 137 NaCl, 5 KCl, 1 $NaH_2PO_4 \cdot H_2O$, 24 $NaHCO_3$, 2 $CaCl_2 \cdot 2H_2O$, 1 $MgSO_4 \cdot 7H_2O$, 11 glucose, pH 7.5). Optimal length (L_0) was found by first performing a tetanus to remove any slack in the sutures, allowing the muscle to recover, and then increasing length until twitch forces plateaued. Force frequency relationship was determined by subjecting muscles to increasing stimulation frequencies (in Hz: 1,10, 20, 40, 60, 80, 100, 150 for soleus with an additional 200 for EDL). Muscles were allowed to recover for 30, 30, 60, 90, 120, 120, 120, 120 s between subsequent stimulations. Force obtained (converted to mN) was normalized to the physiological cross-sectional area (PCSA) through the following equation: PCSA = mass(mg) / [muscle density(mg/mm^3) * fiber length(mm)]. The physiological density of muscle is 1.056 and fiber length was found utilizing a fiber length to muscle length ratio, 0.72 for soleus and 0.51 for EDL (Burkholder, Fingado, Baron, & Lieber, 1994).

GST Pulldown

GST fusions were made using ligation-independent cloning with vector pET His6 GST TEV LIC (2G-T), a gift from Scott Gradia (Addgene plasmid #29707). The cloned SRR and SH3 domains correspond to Uniprot Q9JL90 amino acids 629-715 and 716-768, respectively. DNA templates were prepared from C57BL/6J soleus [RNeasy Fibrous Tissue Mini Kit (Qiagen) for RNA isolation and Superscript III (Invitrogen) for cDNA production]. Amplification of the domains used CloneAmp HiFi Polymerase (Clontech) with primers to the SRR (SRR_F: 5'-*tacttccaatccaatggagga*CGCCGGAGCCGGGACC-3', SRR_R: 5'-*ttatccacttccaat*ACGGAAGATTTTCCCGGCAGTAGACG-3') and the SH3 domain (SH3_F: 5'-

*tacttccaatccaatggagga*GCTATATATGACTATATAGCTGCAGATGCGGATGAAGTGT-3', SH3_R: 5'-*ttatccacttccaat*AATAGCTTCCACATAGTTGGCAGGGAGCATA-3'). Purified PCR products were cloned into SspI-linearized vector using the In-Fusion HD Cloning Kit (Clontech). The products were transformed into Stellar Competent Cells (Clontech) and spread on agar plates (100 µg/mL). Purified construct sequences were confirmed with GST_forward and T7_reverse primers recommended for the vector. To express the protein sequences, vectors were first transformed into Rosetta (DE3)pLysS Competent Cells (Novagen) and grown up in media containing ampicillin (50 µg/mL) and chloramphenicol (34 µg/mL). Protein induction was done in LB lacking chloramphenicol but containing IPTG (1 mM) at room temperature for 3-4 hours. These cells were pelleted and frozen at -80°C pending further use.

To purify the protein constructs, cells were lysed in a lysis buffer [in mM: 20 Tris, 10 imidazole at, 150 NaCl, 2 β-mercaptoethanol, 0.2% NP-40, and a single cOmplete protease inhibitor cocktail tablet (Sigma) per 100 mL H_2O at pH 8.0]. Lysozyme and DNaseI were added to the solution and the cells were broken apart by sonication. The mixture was centrifuged and the supernatant was filtered onto a column containing 0.5 mL Ni-NTA Agarose beads (Qiagen). Once bound, cell supernatant was washed with buffers based on the lysis buffer [5 mL of each: wash 1 (lysis without NP-40), wash 2 (wash 1 with 1 M NaCl), wash 3 (wash 1 with 25 mM imidazole)] before being eluted with 2.5 mL of an elution buffer (wash 1 with 330 mM imidazole). Fractions were analyzed via SDS-PAGE to ensure the purity of the collected GST-tagged construct (GST+SRR: 35.34 kDa, GST+SH3: 31.76 kDa, GST+SRR+SH3: 41.10 kDa).

Finally, pulldowns were performed using glutathione beads (Thermo Fisher) and whole muscle lysate from the TC. Muscles were ground up in a glass Dounce tissue homogenizers before being incubating in a high salt lysis buffer (in mM: 100 $NaHPO_4$,

150 NaCl, 1 PMSF, 0.08 E-64, 0.376 leupeptin, 5 EGTA, 0.4% NP-40 at pH 7.5). Construct-bound glutathione beads were then incubated with the muscle lysate supernatant. After eluting the lysate solution, it was mixed with a low salt lysis buffer (0 mM $NaHPO_4$ instead of 100 mM) to make a 40 mM $NaHPO_4$ medium salt lysis solution. Beads were then incubated twice with additional medium lysis (40 mM $NaHPO_4$ from high and low lysis buffer stocks) buffer for 2.5 hrs each, the flow throughs being pooled together. Post-incubation, beads were washed in medium lysis buffer (5 x 10 min) before baits were denatured and released from the beads using an 8 M urea solution (in M: 8 urea, 0.05 Tris-HCl, 0.150 NaCl at pH 8.0). To run for SDS-PAGE, eluted fractions were mixed in a 1:1 ratio with an SDS running buffer containing bromophenol blue (62.5 mM Tris-HCl at pH 6.8, 2.5% SDS, 0.002% bromophenol blue, 10% glycerol, and 5% β-mercaptoethanol).

IGF-1 AAV

Viral delivery of IGF-I was used to promote muscle hypertrophy. Recombinant self-complement AAV serotype 2/8 was used to facilitate skeletal muscle targeting. The AAV harbored the cDNA sequence for murine class I *Igf-1A*, which allows for better uptake into cells (Barton, 2006). This sequence includes the MHC class I signal peptide, followed by the mature IGF-1 protein, and ending with the E-peptide specific to this IGF-1 isoform. AAV serotype 2/8 was used to facilitate skeletal muscle targeting. The anterior compartment of the lower hindlimb was injected, with the TC being the target of an intramuscular injection and the EDL receiving dosages via diffusion within the compartment. Muscles were injected at five months of age, one leg being treated with 2.47 x 10^{10} viral copies in 50 µL of PBS while the other leg with treated with 50 µL of PBS only. Mice were then sacrificed one month after injection, at 6 months of age.

Following this, both TCs and EDLs were dissected and weighed. Other hind limb muscles were also weighed as negative controls. TCs were flash frozen while EDLs were pinned at slack length and embedded in OCT for cryosectioning.

Exercise testing

We used 6-month-old mice that were individually housed in a 13.9″L × 9.25″W × 7.9″H pan outfitted with a freely rotating 12.7cm diameter wheel with a 5.7cm wide running surface (Lafayette Instruments, Lafayette, IN, USA). Running wheels were connected to a computer that recorded activity in 5s intervals, for a total of 21 days. Mean running time, speed, and duration per 24h period were determined for the last 8 days of the testing period (when running performance was stable). The mice were provided food and water ad libitum under a 12:12 h light/dark cycle.

Statistical Significance

All data presented in this dissertation are represented as mean ± SEM. For all experiments comparing two groups of data, Mann-Whitney t-tests were performed following confirmation that numbers were insufficient to assume normal distributions where $p < 0.05$ was considered significant. In experiments that had multiple variables, two-way ANOVA was used with Tukey *post hoc* tests corrected for multiple comparisons ($p < 0.05$ significance). In all data presented, the following symbols are representative of significance: *, **, ***, **** for $p < 0.05$, $p < 0.01$, $p < 0.001$, $p < 0.0001$ respectively.

Chapter 3: Results

Aim 1: Characterization of Conditional Nebulin Knockout Mouse Model

Basic Conditional Knockout Model Characterization

In studying the conditional nebulin knockout (Neb cKO) mouse model, it was immediately apparent that there was a severe myopathic phenotype occurring. Knockout mice appeared to be distinctly smaller than their littermates (Figure 6). Even by the one-week time point, these mice were immediately identifiable through size and movement. There was also a significant number of knockout mice that died as mice aged, resulting in a high mortality until around three months of age. Past this time point, it appeared that Neb cKO mice survived much better, yet still retained a severe weight deficit. These deficits were in part due to severe weight loss in multiple limb muscles (Figure 7). Studying muscle weights at 3 weeks, 5 weeks, and 6 months revealed a variety of changes. Specifically, in the gastrocnemius and quadriceps, weights started out approximately 60% lighter than the control tissues and only got worse with time. The TC, EDL, and diaphragm each seemed to lose a bit of weight at the 5-week time point but regained the weight by 6 months. Finally, the soleus exhibited a significant amount of hypertrophy by the 6-month time point. When viewed side-by-side with control muscles, there was also a distinct color change in the knockout tissues, pointing towards protein composition changes. Together, these data showed that Neb cKO mice were experiencing severe body weight loss and significant, but muscle-specific muscle, weight loss that was together having a detrimental effect on survival and development.

Figure 6: Growth and Survival of Neb cKO Mice

A) Conditional knockout mice have an immediate weight deficit that remains apparent through adulthood. B) These mice have a high rate of mortality that affects developing mice in the first three months of life. Past the three-month time point, mice appear to stabilize and the death rate declines sharply.

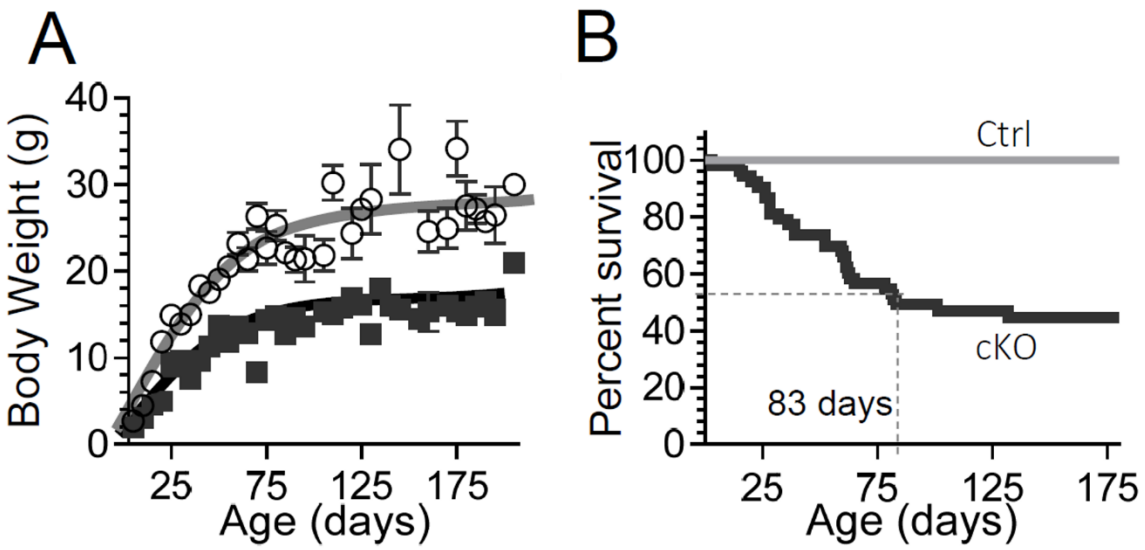

Figure 7: Severe Muscle Weight Loss in Neb cKO Mice

Quantification of limb muscle weights over multiple time points. A) Weight deficits compared to control values. Significant weight loss observed in TC, EDL, Gastrocnemius, and Quadriceps. However, a significant hypertrophy was noted in the soleus. B) Comparison of control and knockout tissues. Nebulin knockout muscles have a distinctly redder hue. (Scale Bar: 5mm)

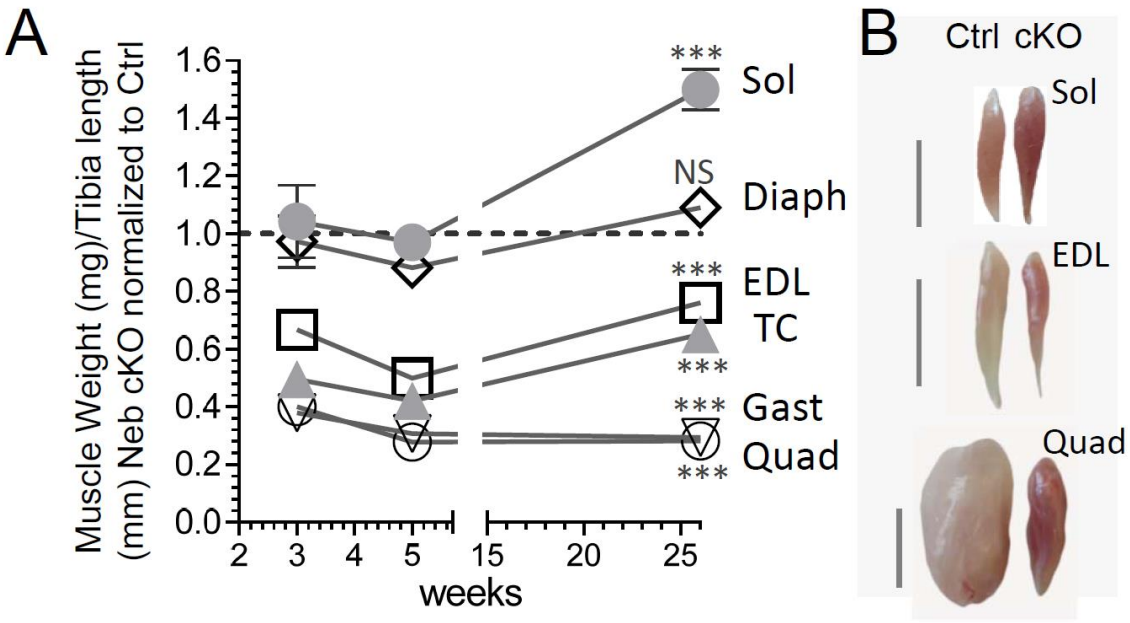

Quantification of Protein Expression

The removal of nebulin from the muscle sarcomeres was quantified via western blot (Figure 8). Studies revealed a significant reduction in nebulin protein expression. At the earliest characterized age of 3 weeks, the average nebulin level was 48% of Ctrl levels, at 5 weeks 4.8% and at 6 months 2.2%. This demonstrates the effectiveness of the MCK-Cre transgene and confirms that this model is a nebulin knockout model.

Study of MHC Isoform Composition

MHC isoform expression was studied using gel electrophoresis to better understand the compositional changes implicated in observations made during basic characterization of this model (Figure 9). MHC type I and IIB are well separated on gels (bottom and middle bands, respectively), while the top band consists of a mix of IIA and IIX proteins. Attempts to separate IIA and IIX bands were not successful and the analyzed band is referred to here as IIA(X). MHC composition in control and Neb cKO samples was quantified at three time points. Interestingly, the diaphragm showed a minimal change in composition while all other muscle types shifted towards slower fiber types, namely type I and IIA(X). In the soleus, type I fibers became more prominent at the expense of type IIA(X) and in the other muscle types both type I and IIA(X) were increased at the expense of type IIB fibers. Additional experiments correlating IIB content and muscle loss also showed that there was a correlation between type IIB content and the amount of atrophy the muscle went through (Li et al., 2015).

Figure 8: Quantification of Nebulin Expression

Nebulin expression was quantified via western blot and an antibody to the N-terminus. (Top) A representative blot made at 5 weeks. Contrast was enhanced to emphasize the residual N-terminal signal in the knockout tissues. (Bottom) Protein expression expressed over three time points. In each muscle group, the decrease of expression following MCK-Cre expression at birth can be visualized. By 5 weeks, muscles have nearly reached a minimal level of nebulin expression.

00

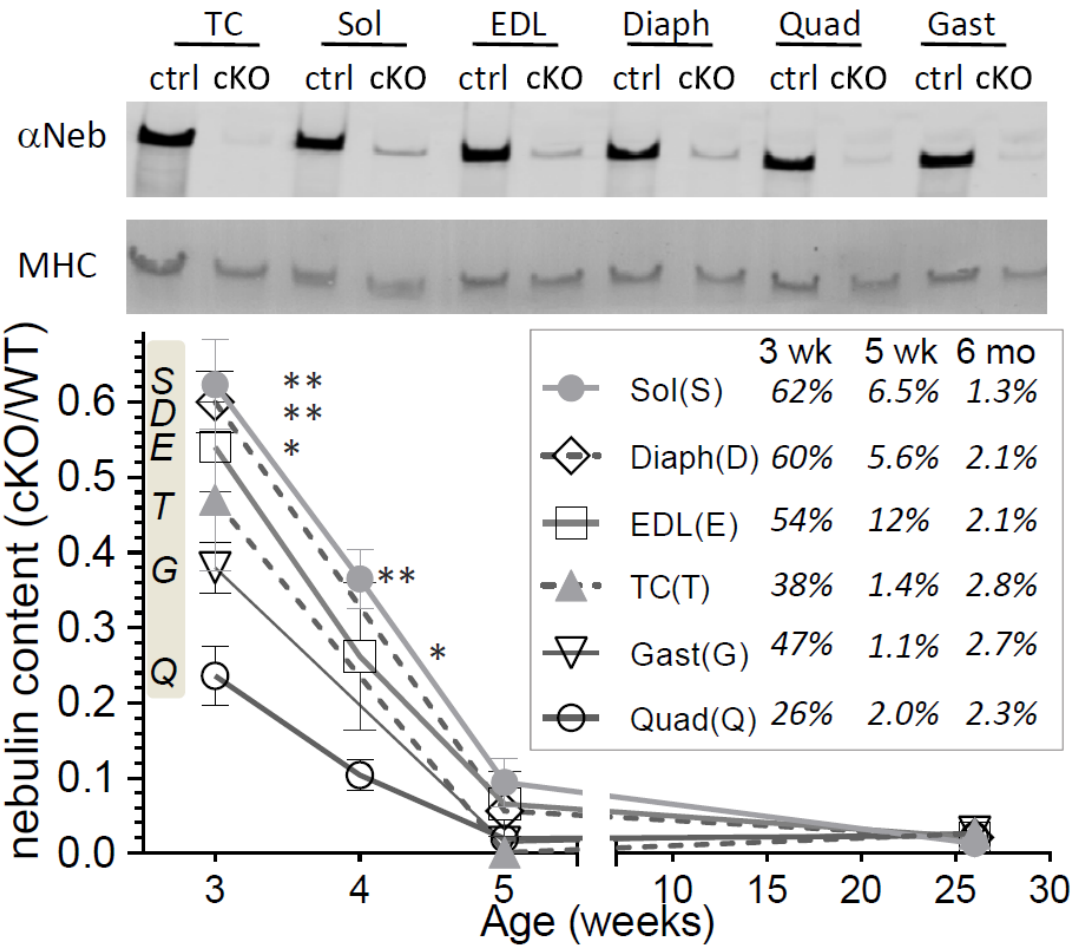

Figure 9: MHC Composition of Limb Muscles

MHC isoform was quantified through gel electrophoresis. A) Representative gel of MHC isoform separation. Due to complications in the technique, separation of IIA and IIX bands was unattainable and the merged band was labeled IIA(X). B) Expression over time represented as a % of total MHC in that specific sample. Shifts to slower fiber types represented as increasing proportion of pink and red bars.

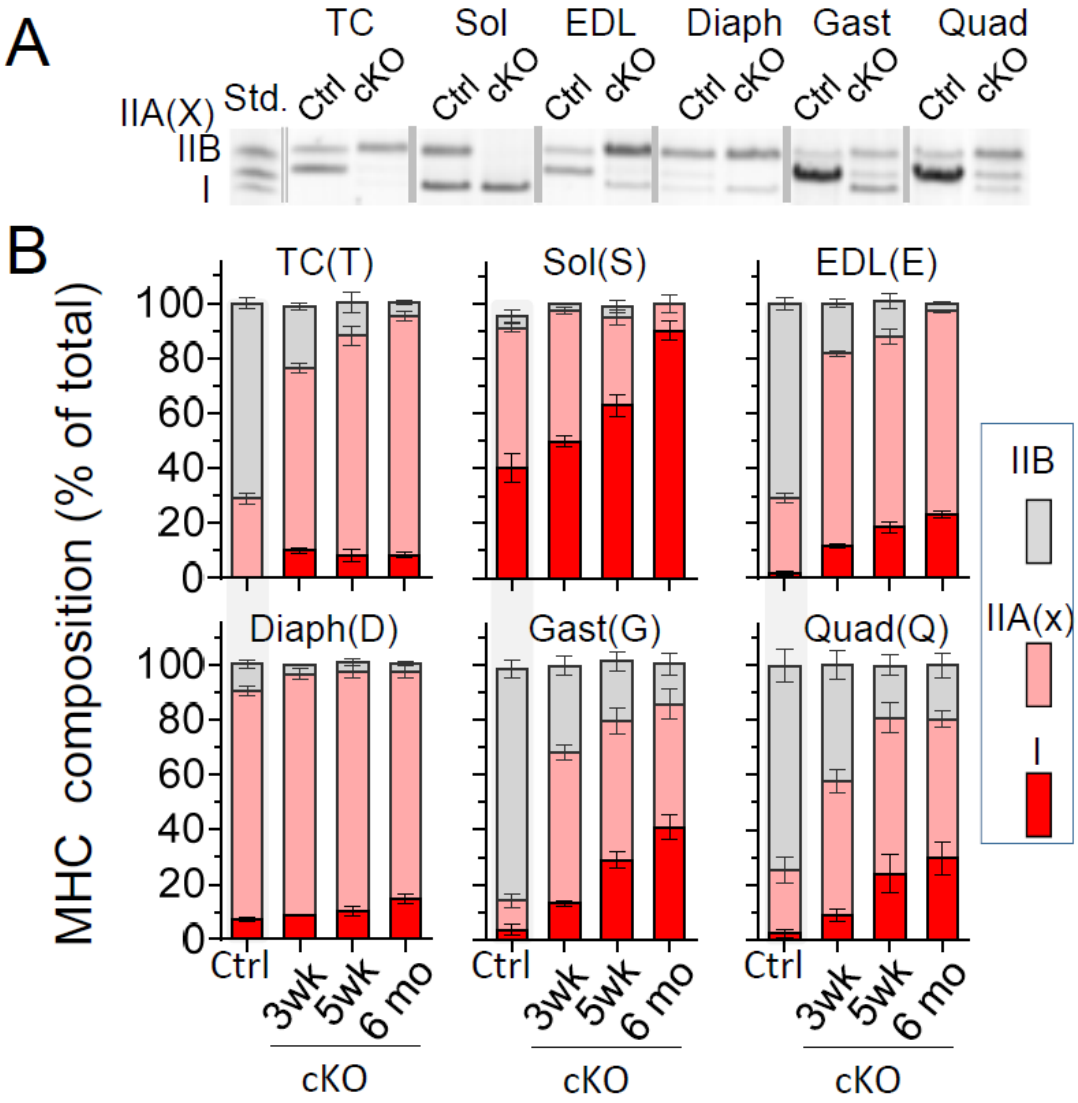

Quantification of Force Production

Testing of functional performance of the Neb cKO mice was done using by providing 6-month-old mice access to a free-running wheel and measuring the average 24h running duration, speed, and distance. Neb cKO mice did exercise, but at a reduced rate compared with Ctrl mice (Figure 10). There was a reduction in duration (1.2 versus 5.4 h), speed (0.4 versus 1.1 km/h), and distance ran (0.5 versus 6.6 km). This reduced exercise performance suggests compromised muscle function. *In vitro* studies were therefore performed on intact EDL and soleus muscle, selected for their suitability for this type of work and their glycolytic (type IIB) and oxidative (type I and IIA) fiber-type predominance, respectively. Muscles were dissected from 5-week- and 6-month-old mice and, following electrical stimulation, the produced force was measured. The soleus of NEB cKO mice produced normal maximal tetanic forces compared with controls, whereas in EDL muscle tetanic force levels were 80–90% reduced. We determined the CSA of the studied muscles and used this to calculate specific force (force divided by area). Specific force levels were significantly reduced at both ages and in both muscle types indicating that nebulin deficiency reduces the force-generating capacity of skeletal muscle.

Figure 10: Force Deficits in Neb cKO

Nebulin deficiency hinders running performance and lowers specific force of isolated muscles. A) Neb cKO mice (6 months) are active on a free-running wheel but running duration, speed and distance are greatly reduced relative to age-matched Ctrl mice. B) Examples of maximal tetanic force traces superimposed for the two genotypes (6 months) in soleus (left) and EDL muscle (right). C) Mean tetanic force is unaltered in soleus (left) but severely reduced in EDL (right). D) Maximal specific force (force divided by CSA) is reduced in soleus as well as EDL.

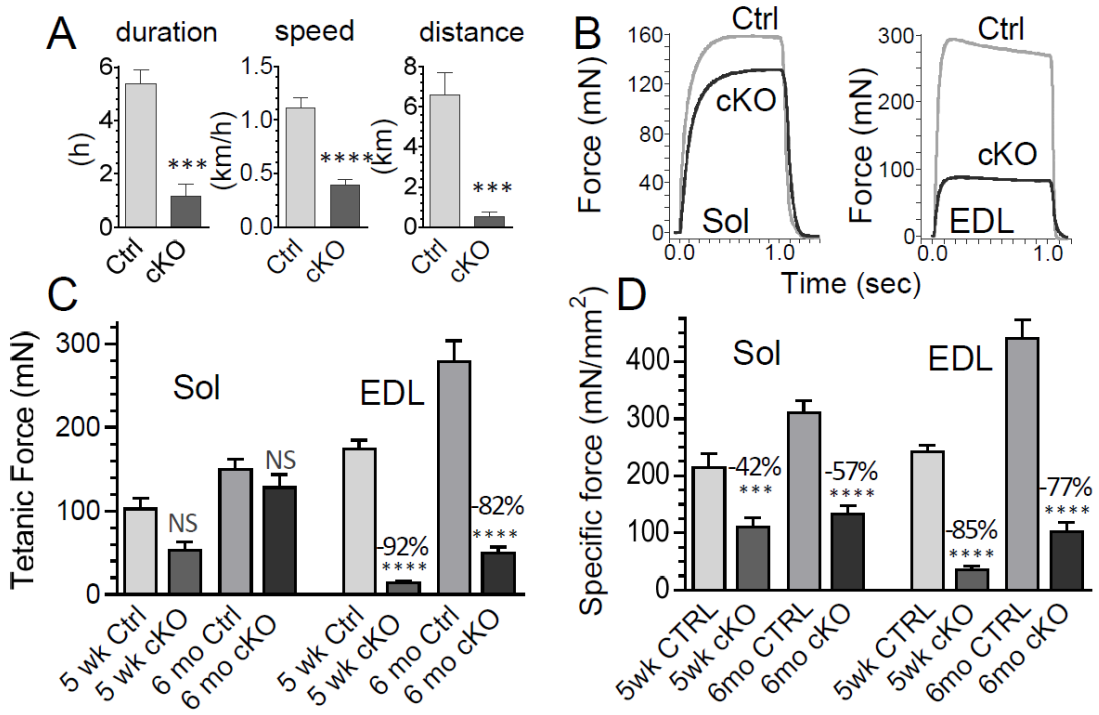

Aim 2: Characterization of Nebulin Truncation Mouse Model

Basic Characterization of the Neb$^{\Delta 163\text{-}165}$ Model

To investigate the role of nebulin's unique C-terminal domains in the skeletal muscle sarcomere, a mouse model which would produce a nebulin protein lacking the serine-rich region (SRR) and the SH3 domain was generated. In order to remove those domains from the endogenous *Neb* locus, homologous recombination was performed using a vector containing a series of stop codons followed by an FRT-flanked neomycin cassette. The location of these stop codons after the start of murine exon 163 allowed for the complete translation of the final actin-binding module, M206 (Figure 2). Flp recombination was used to remove the neomycin cassette and the integration of the stop codons was verified via PCR analysis. Within the first week, it was visibly apparent that there was a weight deficit in the homozygous mice. This deficit carried through into adulthood and mice remained significantly lighter than their wild-type counterparts even at one year of age (Figure 11). However, the truncation of nebulin also had a significant impact on the postnatal survivability of the homozygous mice, resulting in 10% of the total population being homozygous when genotyped approximately ten days after birth. This skewed Mendelian ratio is likely due to deaths within the first week of life as the distribution of embryonic genotypes was normal and few deaths were ever observed past the one-week time point. Despite the initial high mortality rate, 87% of surviving homozygous mice survived to adulthood. Interestingly, a comparison of tibia lengths in these mice revealed no significant changes, suggesting that the weight loss observed was not due to an inherently smaller mouse. In summary, we created a mouse model lacking the two C-terminal nebulin domains in which homozygous mice live to adulthood and the *in vivo* functions of the SRR and SH3 domain can be studied.

Figure 11: Basic Characterization of Neb$^{\Delta 163\text{-}165}$

Mice producing a truncated nebulin have significant weight deficits and changes in survival. A) Mouse weight comparison at three different time points (male n=5,5,4, female n=12,8,5). Homozygous mice remain lighter through adulthood. B) Postnatal survival (n=97). Postnatal deaths were observed as early as one week of age. C,D) Distribution of genotypes in embryonic and postnatal mice from Het-Het breeding pairs (postnatal n=1023, embryonic n=101). Postnatal genotypes significantly different from Mendelian ratios.

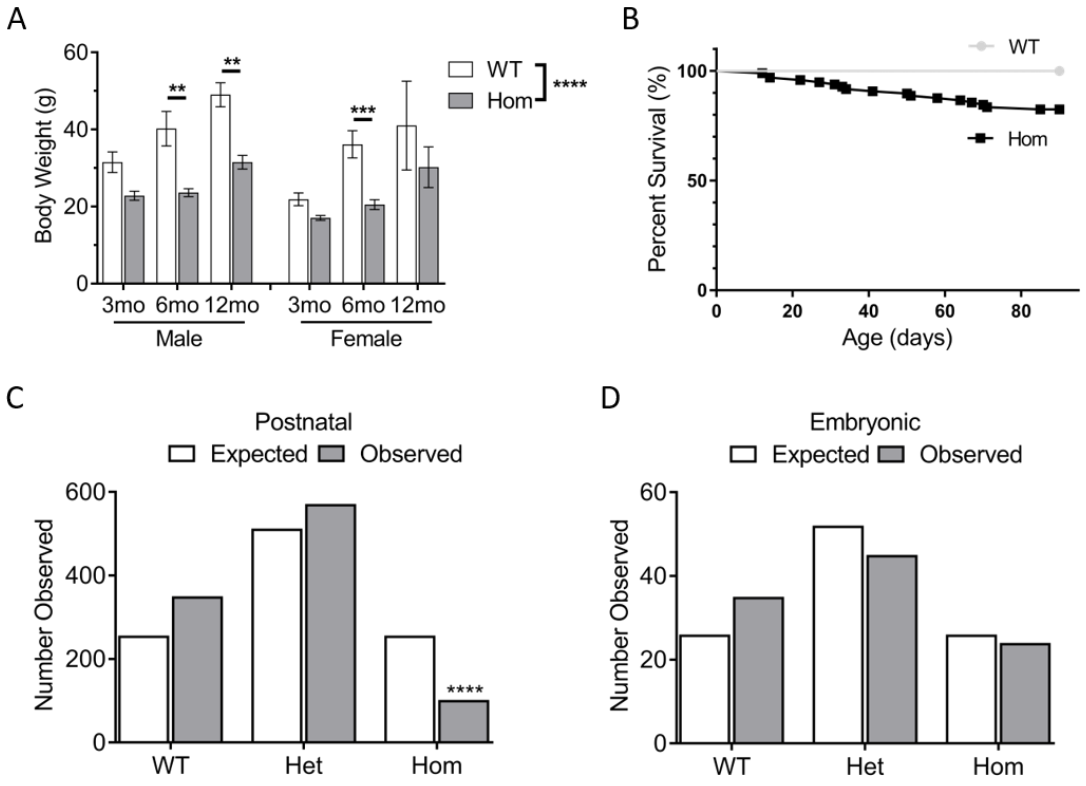

Muscle Weight Changes and MHC Distribution

Analysis of distal limb muscles revealed that several had decreased weights compared to wild-type, especially in the gastrocnemius, plantaris, and quadriceps where weights were reduced by ~50% (Figure 12). These deficits persisted through adulthood and despite a slight lag in homozygous muscle weight at 6 months, limb muscle weights remained at a constant ratio to wild-type weights, returning to the same ratio by 12 months. In performing gel electrophoresis on multiple limb muscles, every muscle studied was found to have a significant shift in their MHC fiber type composition (Figure 13). The shift trended towards slower fiber types, resulting in a reduced ratio of IIB fibers and increased IIA/X and I fibers. Even muscles that did not originally have a prominent type I fiber population, such as the EDL, gained a small population of those fibers.

Importantly, muscles that did not display a weight reduction, such as the soleus and the EDL, both experienced this compositional shift. To better understand these changes in the absence of an overt weight deficit, the changes occurring in individual fiber types that likely accompanied this shift were investigated. Specifically, the EDL was studied due to the appearance of the Type I fibers, which do not normally exist in this muscle. Here it was found that there was a significant increase in the number of fibers in the homozygous EDL, with both IIX and IIB fibers experiencing significant increases in fiber count. However, despite having more fibers, IIB fibers account for a smaller fraction of the whole cross-sectional area, while the area covered by IIX fibers increases. Slower fiber types such as Type I and IIA experience an increase in fiber size but neither appears to contribute significantly to the maintenance of the EDL weight. Conversely, faster fiber types become smaller. These data show that it is a combination of hyperplasia of the IIB and IIX fibers as well as retention of Type IIX fiber size that results in the homozygous EDL matching the wild-type EDL in overall weight.

Figure 12: Neb$^{\Delta 163\text{-}165}$ Muscle Weight Changes

Multiple limb muscles have weight deficits. A,B) Muscle weights at 3 months (n=9-10). Raw values are normalized to tibia length. Relative weights obtained by normalization to wild-type averages. C) Muscle weight deficits observed throughout homozygous lifespan (n=9,6,4). 2-Way ANOVA reveals age has a significant effect on the diaphragm ($p<0.0001$), with soleus trending ($p=0.06$) and EDL being not significant ($p=0.3$).

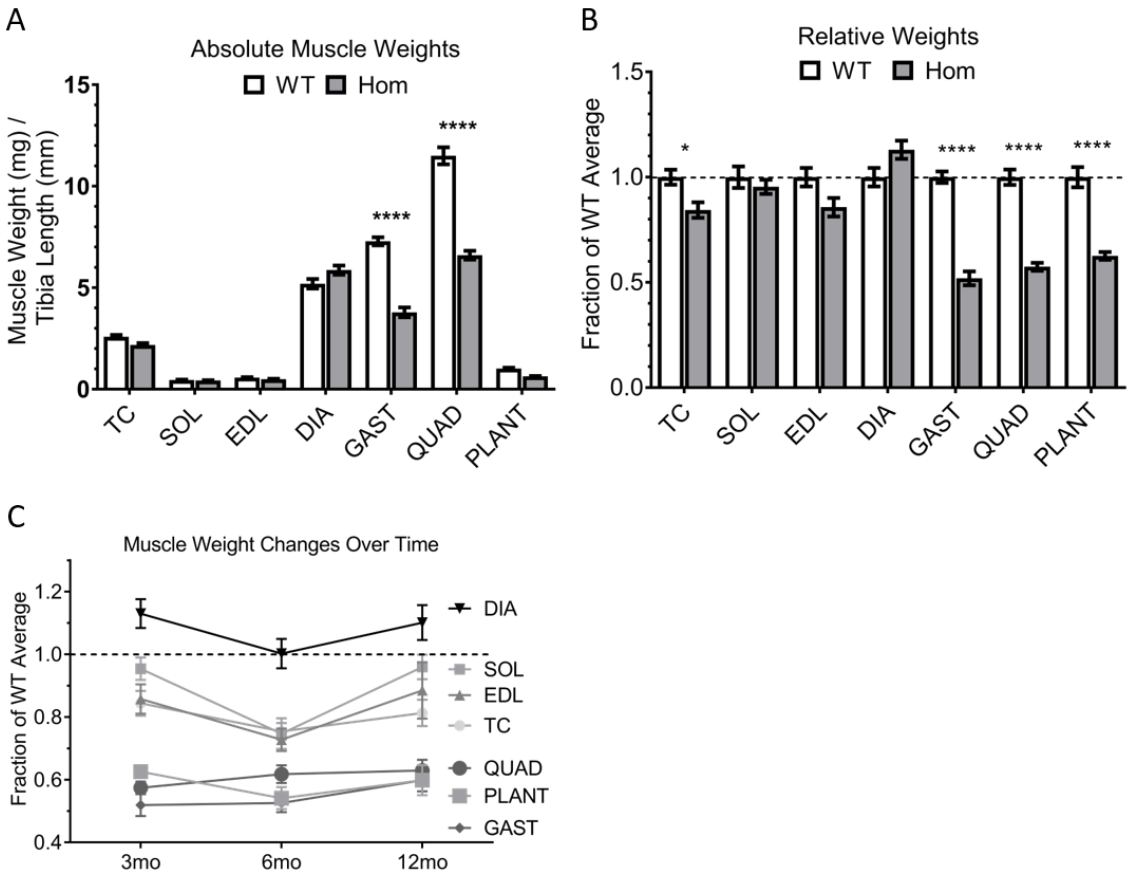

Figure 13: Neb$^{\Delta 163\text{-}165}$ MHC Distribution

MHC isoforms shift towards slower fiber types, though some muscles attempt to compensate for the changes. A) Representative acrylamide gel of MHC fiber type ratios in both wild-type and homozygous mice. Control sample is a mix of TC and SOL from C57BL/6J mouse. B) Graphical representation of changes in ratios between wild-type and homozygous mice (n=12). Shift to slower fiber types indicated by increasing fractions of both Type IIA/X and Type I. C) Distribution of different fiber types in the EDL muscle (n=9,7). IIB and IIX fibers are significantly greater in the homozygous tissue. D) Area covered by different fiber types in the EDL muscle (n=9,7). IIB area is significantly reduced while IIX area is significantly increased. E-H) Changes in minimum Feret diameter of fiber types in the EDL muscle.

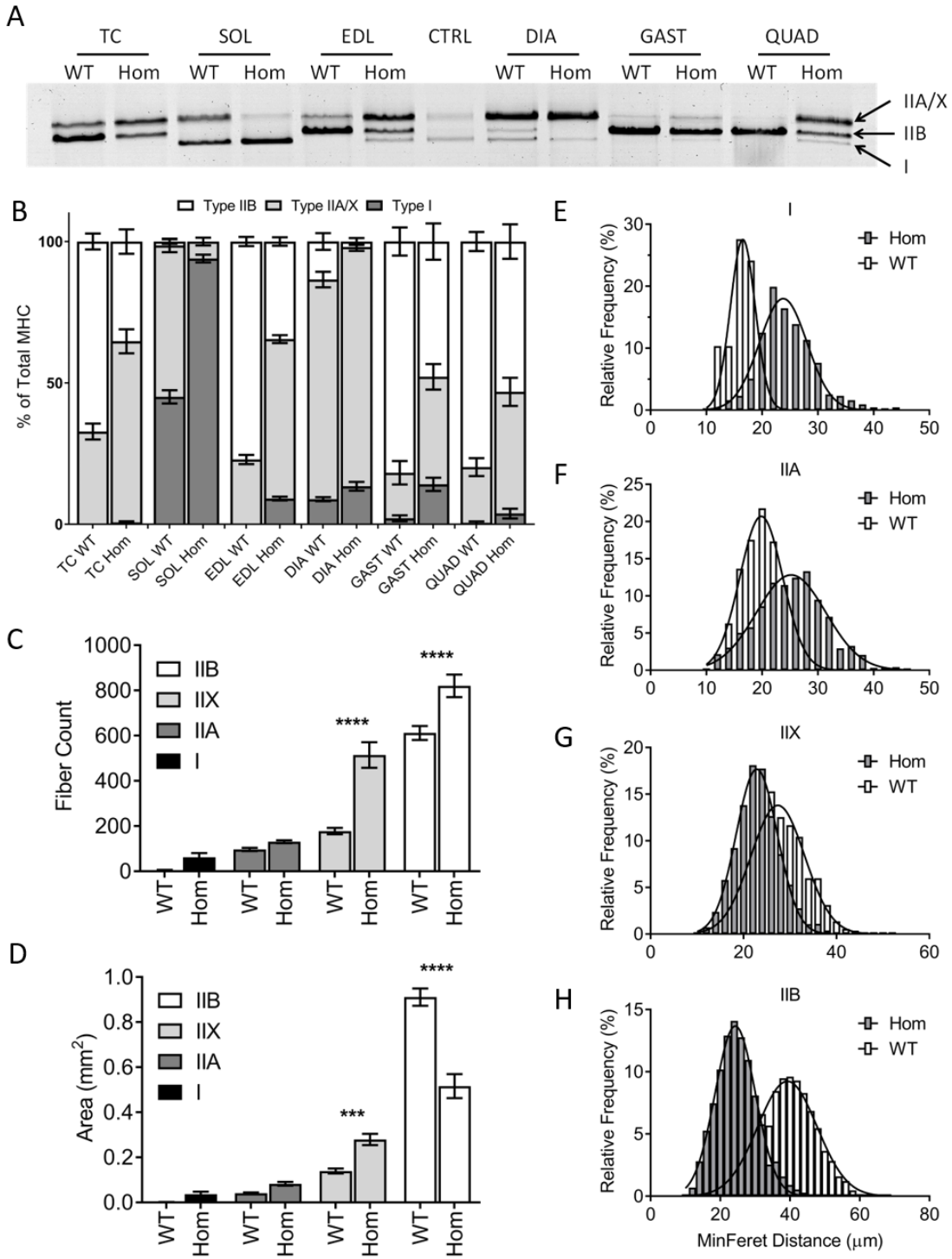
A
TC
SOL
EDL
CTRL
DIA
GAST
QUAD
WT
Hom
IIA/X
IIB
I
B
Type IIB
Type IIA/X
Type I
% of Total MHC
TC WT
TC Hom
SOL WT
SOL Hom
EDL WT
EDL Hom
DIA WT
DIA Hom
GAST WT
GAST Hom
QUAD WT
QUAD Hom
C
Fiber Count
IIB
IIX
IIA
I
****
D
Area (mm2)
***
E
I
F
IIA
G
IIX
H
IIB
Relative Frequency (%)
Hom
WT
MinFeret Distance (μm)

Variations in Protein Expression and the Retention of Thin Filament Length Regulation

To determine how well the truncated nebulin was being transcribed and translated, western blots were performed on different limb muscles using antibodies to the N- and C-terminus of nebulin. It was found in the homozygous mice that while the N-terminus was intact, as expected the SRR and SH3 domains were missing (Figure 14). Those results further confirmed the proper truncation of the protein. However, due to limitations in the 0.8% agarose gel used, there was insufficient resolution to visualize the ~15kDa change in molecular weight. Quantification of N-terminal expression revealed that several muscles had reduced protein expression. This protein deficit in homozygous tissues was observed at multiple time points, but that deficit did not significantly change throughout those time points. Surprisingly, the homozygous soleus maintained wild-type levels of protein expression. Quantification of the mRNA transcript using qRT-PCR showed that in fact there was a persistent deficit of nebulin transcript in all limb muscles, including the soleus. This indicates that the truncation of nebulin's C-terminus is affecting the stability of the mRNA transcript and may be playing a role in the decreased protein expression.

Figure 14: Nebulin Protein and mRNA Expression

Limb muscles have deficits in protein and mRNA expression, but the soleus still produces normal amounts of nebulin. A) Representative western blot utilizing several hind limb muscles. Truncation confirmed through SH3 antibody due to complete absence of signal. B) Quantification of nebulin protein expression through N-terminal antibody signal and normalized to MHC content over multiple time points (n=8,8,6). Soleus expression is comparable to wild-type. Two-way ANOVA shows age has no effect on protein expression in homozygous soleus. C) Quantification of mRNA expression in TC, soleus, and EDL.

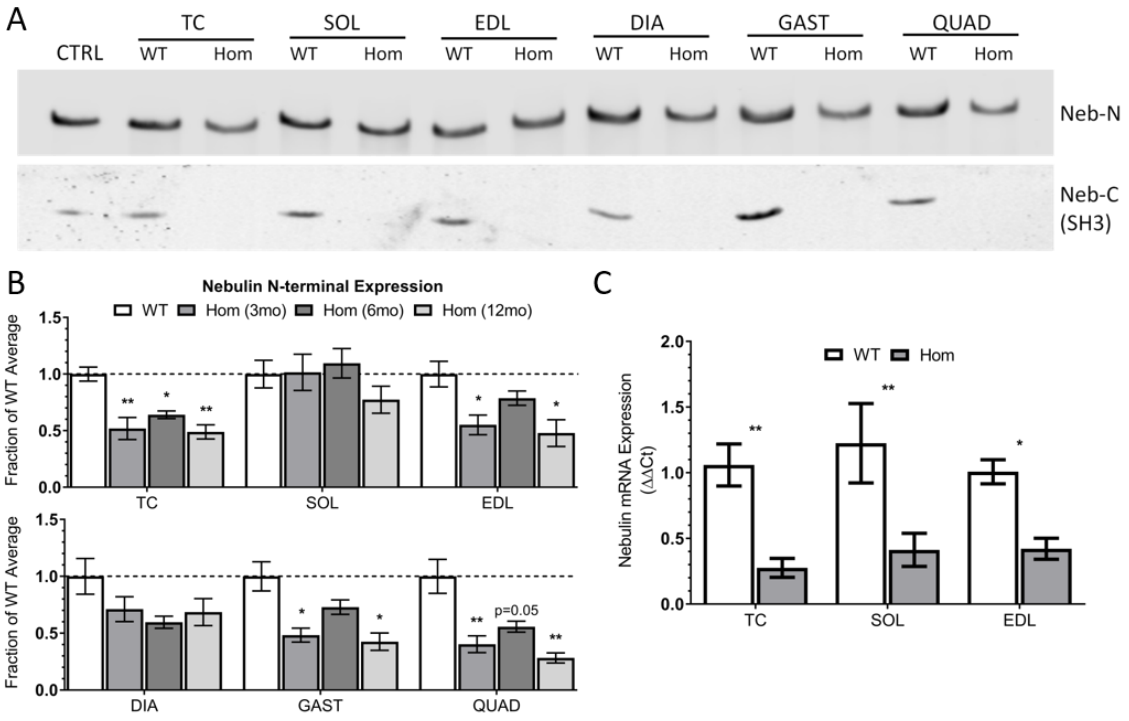

Despite the truncation, nebulin was still able to insert into the Z-disk. Domains near the truncation were localized in the Z-disk using an antibody to modules 197 through 202 (originally referred to as M176-181), with the final actin-binding module (M206) being only four domains away (Figure 15). Additionally, nebulin was still able to localize properly to the thin filaments, with the N-terminus forming an expected doublet near the H-zone of the sarcomeres. These data show that nebulin still aligns with the thin filaments. This was further supported by the observation that thin filament lengths in both the soleus and the EDL were not significantly different between wild-type and homozygous mice. These findings indicate that while the loss of the C-terminus affects protein stability during translation, nebulin has nevertheless retained its ability to regulate the thin filament lengths.

Figure 15: Nebulin Localization and Thin Filament Length Regulation

Nebulin is properly localized and thin filament lengths are normal. A) Diagram of antibody locations. The section of nebulin embedded within the Z-disk is identified. B) Localization of modules M197-202 (α-M176-181, red) in EDL along with phalloidin (green) and α-actinin (blue). Modules colocalize with α-actinin at the Z-disks. (Scale Bar: 5µm). C) Localization of nebulin in the sarcomere utilizing the nebulin N-terminal antibody (red) and an α-actinin antibody (blue) to identify the Z-disks. Doublet near the H-Zone of the sarcomere was identified as nebulin. (Scale Bar: 5µm). D) Thin filament length comparison in soleus and EDL. Soleus is not significantly different, EDL trends to slightly longer thin filaments (p=0.06) (n=4,6,9,7).

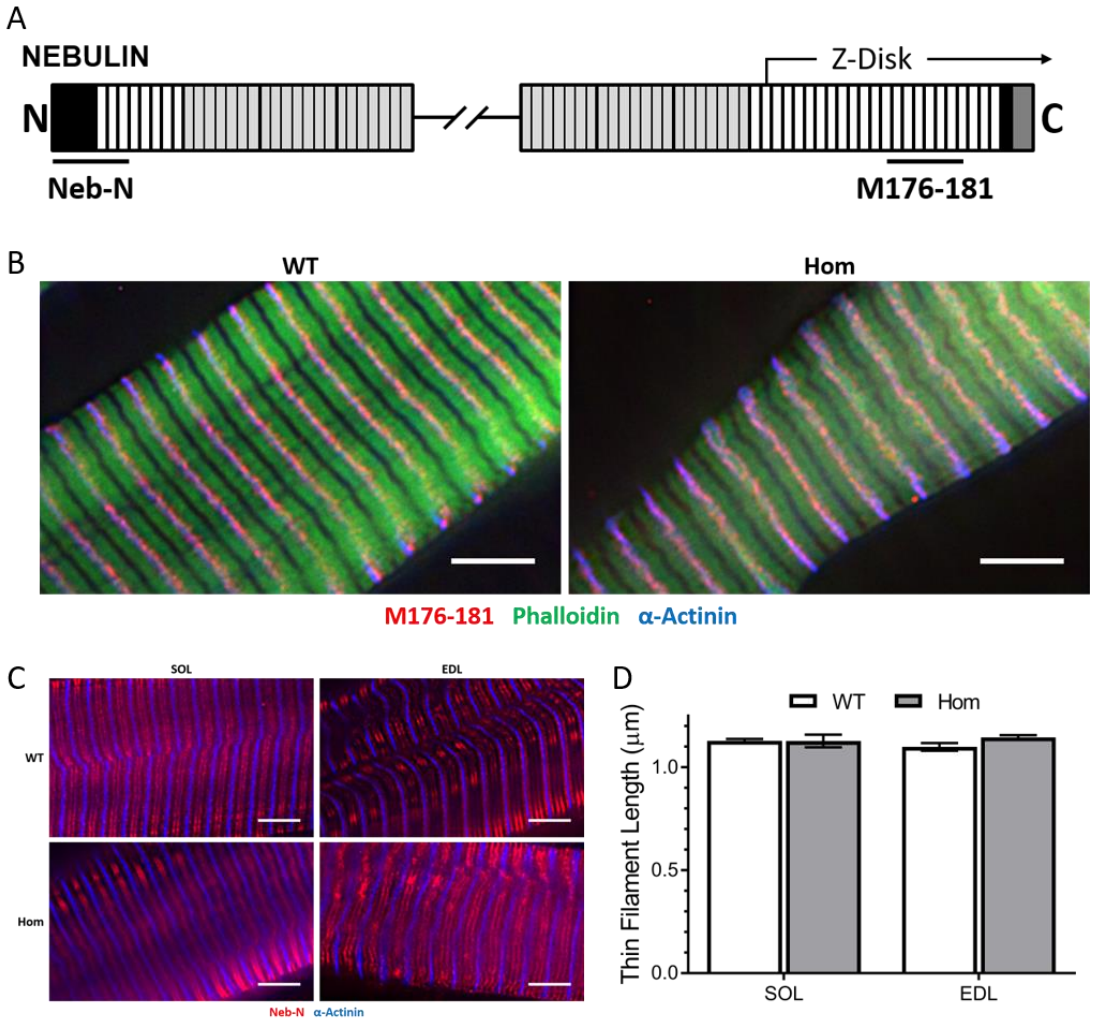

Effects on Sarcomere Structure and Z-disk Width Regulation

To test the hypothesis that loss of the C-terminus is sufficient to induce the mild myopathic phenotype observed, namely the partial weight deficits and fiber-type switching, limb muscle structure and function was studied. Again, the soleus and the EDL, two functionally opposing muscles, were used with the soleus representing a slow-twitch muscle and the EDL representing a fast-twitch muscle. The sarcomeres of both muscle types were analyzed using electron microscopy. Protein aggregates were found in both muscles, with the EDL exhibiting a more severe phenotype (Figure 16). These aggregates, commonly referred to as nemaline rod bodies (North, Laing, & Wallgren-Pettersson, 1997), were largely found in line with the Z-disks and disrupt the organization of the sarcomeres. Quantification shows that on average, the soleus contained larger rod bodies than the EDL, but those occurred with lower frequency, resulting in less total sarcomeric area being occupied by protein aggregates. In general, the soleus appears less affected by the truncation and presents healthier sarcomeres.

It was also noted in the homozygous muscles that Z-disk widths from aggregate-lacking sarcomeres appeared different, especially in the EDL. When multiple fibers in these two muscles were analyzed, the soleus exhibited a small but significant decrease while the EDL exhibited a large increase in Z-disk widths. These data could both be explained by a combination of the MHC fiber composition changes observed and the loss of nebulin's C-terminus. While wider Z-disks are associated with slower fiber types (Luther, 2009), the loss of nebulin's C-terminus may also influence the width of the Z-disks to a small degree, leading to the changes seen in the soleus. However, because the EDL is a fast-twitch muscle and has much thinner Z-disks compared to the soleus, the shift to slower fiber types is dominant as reflected in the drastic widening of its Z-disks.

Figure 16: Changes in Sarcomere Structure

Protein aggregates are found within all homozygous tissues, regardless of how healthy they appear in terms of overall weight. A) Low magnification view of fiber bundles (Scale Bar: 25μm). Protein aggregates (white arrows) observed frequently in EDL, infrequently in soleus. B,C) Quantification of rod body presence throughout individual fibers (soleus n=20, EDL, n=29). Data was quantified over unique images spread across those individual fibers (soleus n=102, EDL n=135). While EDL contains smaller protein aggregates, they are more frequent and cover significantly more of the fibers. D,E) Examples of sarcomeres without Z-disk aggregates in homozygous mice of soleus and EDL compared to wild-type (Scale Bar: 1μm). Homozygous EDL Z-disks have a distinct widening compared to wild-type. F,G) Quantification of non-aggregate Z-disk widths in soleus and EDL (n=11-29 unique fibers). Soleus exhibits a slight but significant decrease in widths while EDL exhibits a drastic increase in widths.

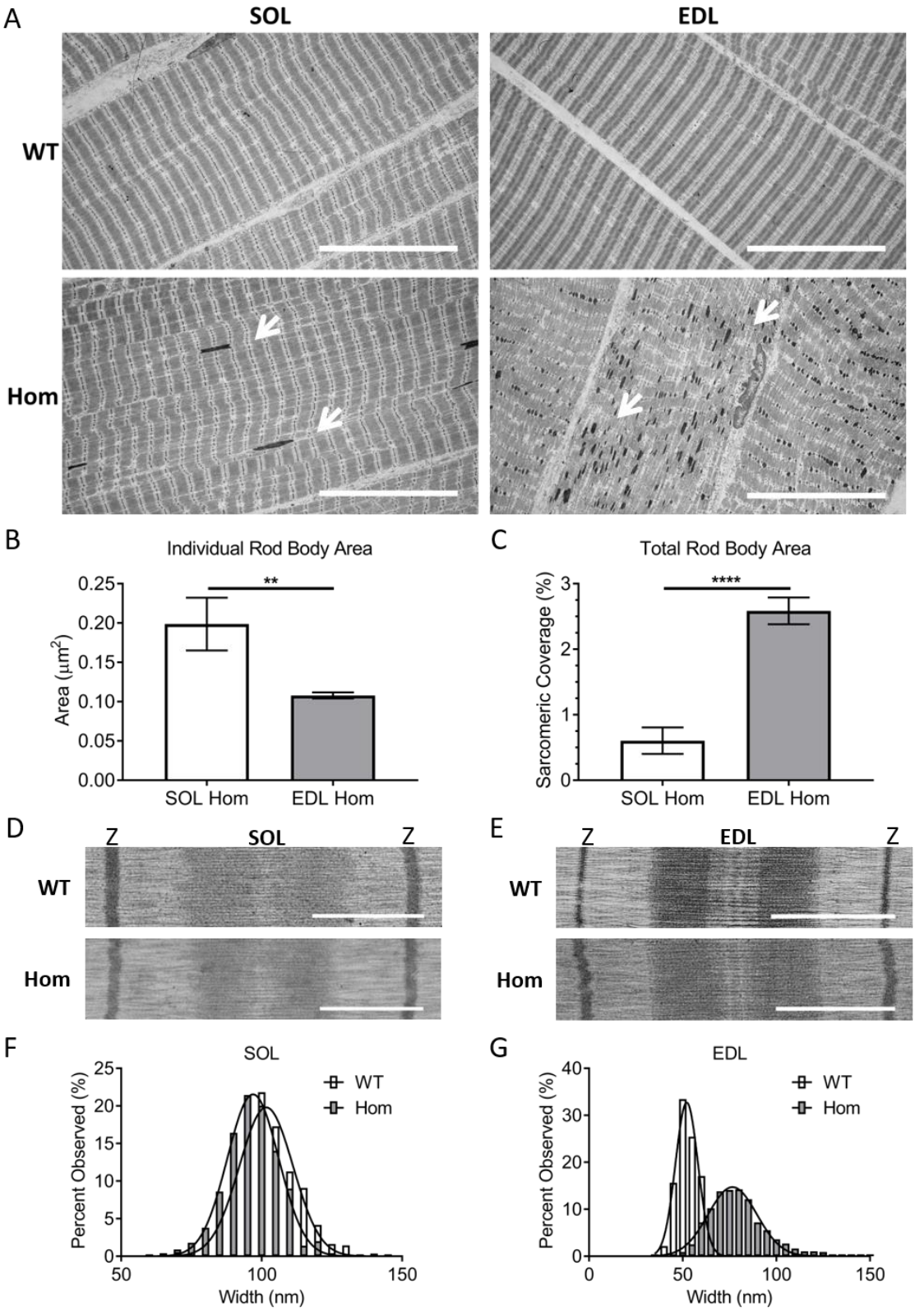
A
SOL
EDL
WT
Hom
B
Individual Rod Body Area
**
Area (μm²)
0.25
0.20
0.15
0.10
0.05
0.00
SOL Hom
EDL Hom
C
Total Rod Body Area
****
Sarcomeric Coverage (%)
3
2
1
0
SOL Hom
EDL Hom
D
Z
SOL
Z
WT
Hom
E
Z
EDL
Z
WT
Hom
F
SOL
WT
Hom
Percent Observed (%)
25
20
15
10
5
0
50
100
150
Width (nm)
G
EDL
WT
Hom
Percent Observed (%)
40
30
20
10
0
0
50
100
150
Width (nm)

Effects on Muscle Contractility

In quantifying the contractility of both EDL and soleus using force-frequency protocols on isolated muscle, it was found that while the EDL displayed a drastic loss of force, the force loss in the soleus was much more subtle (Figure 17). Using two-way ANOVA while considering force production over multiple time points, the homozygous soleus did in fact have a significant force loss. Additionally, while the homozygous EDL muscle could contract and relax in the same amount of time as the wild-type muscle, deficits were noted in the soleus, specifically in the time it took for the muscle to complete a single twitch and the time it took to relax after a tetanus (Figure 18). Considering the normal muscle weight and protein expression of the soleus, these data suggests that the loss of nebulin's C-terminus contributes to slight deficits in contractility observed in this muscle.

Earlier work by Yamamoto et al. showed that the removal of nebulin's SH3 domain resulted in increased sensitivity to eccentric contraction (EC) damage, but did not cause other phenotypes (Yamamoto et al., 2013). The same stimulation-and-stretch EC injury protocol was performed on the largest head of the EDL muscle, known as the fifth-toe EDL, and experiments found a similar trend towards lower forces post-EC damage. However, the inherent force deficit in whole EDL, detailed above, decreased the accuracy of the quantification and only a trending association towards increased EC damage was observed (Figure 17, Bottom). More prominently, the homozygous EDL had a higher rate of force loss from the EC injury protocol (Figure 18, Bottom). Overall, these results support the findings that loss of the SH3 domain results in an increased sensitivity to EC-induced injury and shows that the loss of the SRR in addition to the SH3 domain leads to significant force deficits.

Figure 17: Functional Studies

Both soleus and EDL have reduced force production. A,B) Force-frequency relationship of the soleus and EDL at 3 months. Slight reduction of half-max frequency in the soleus not observed at any other time point or in the EDL. C,D) Max stress produced by the soleus and EDL at various time points (soleus n=8,6,7; EDL n=7,4,6). 2-Way ANOVA indicates the slight decrease in soleus is significant. E) EC injury protocol (n=10). Similar to homozygous whole EDL, the fifth-toe EDL muscle exhibits a significant force drop in baseline tetanus. F) Percent loss in muscles were calculated using an average of the pre-injury forces and the 4th and 5th post-injury forces (n=10). Only a trending significance could be found due to the inherent force deficit in homozygous EDL.

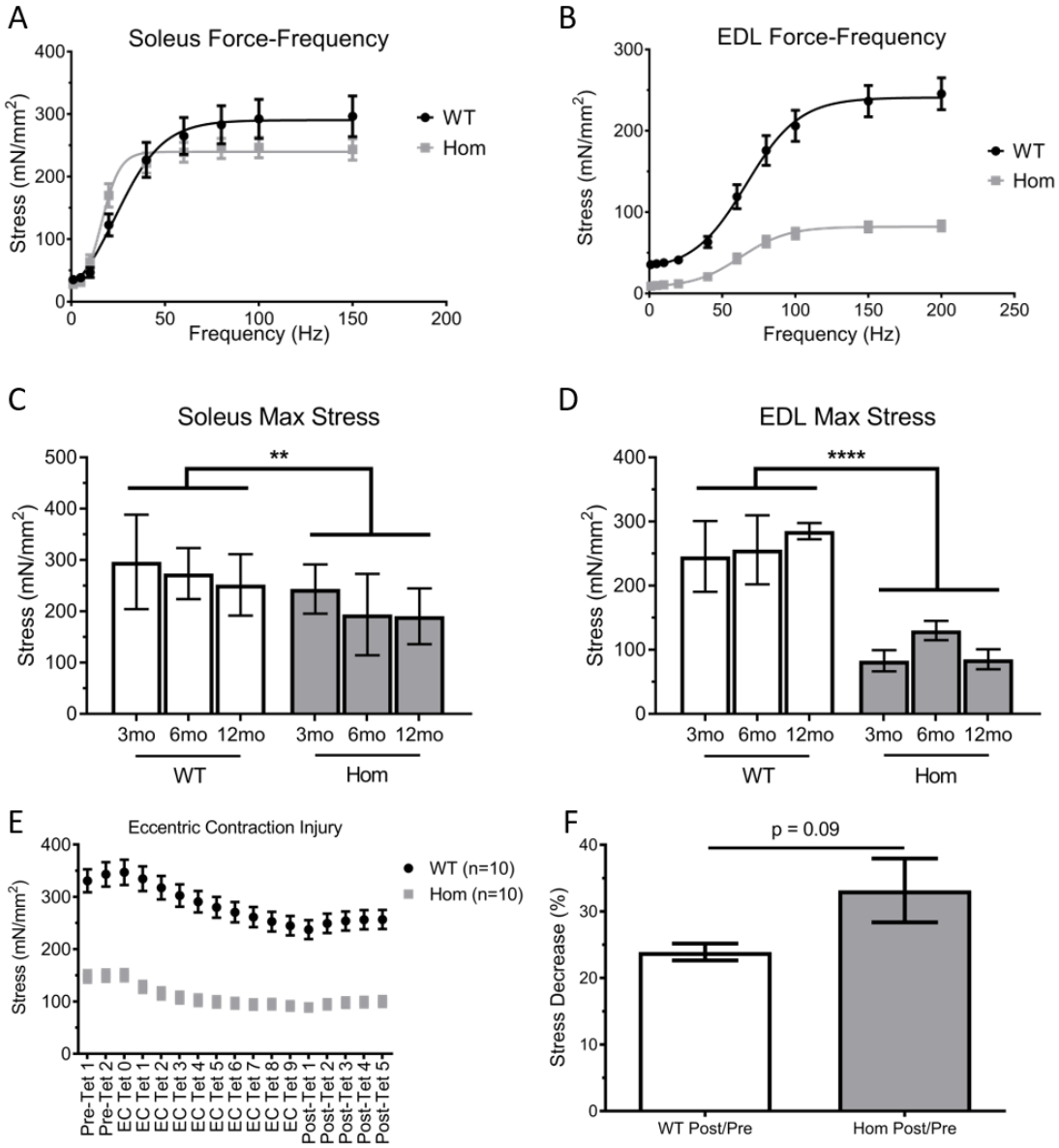

Figure 18: Supplementary Functional Analyses

A,B) Time to max force in soleus and EDL for both twitch and tetanus (n=7-8). Soleus takes significantly longer to produce a twitch but behave similarly to wild-type during tetanus. C,D) Half-Relaxation time in soleus and EDL for both twitch and tetanus (n=7-8). Soleus takes longer to relax after tetanus. Slight differences in twitch relaxation found to be not significant. E) Comparison of EC injury force loss between wild-type and homozygous fifth-toe EDL (n=10). Homozygous tissue loses force exponentially faster than wild-type during the injury protocol.

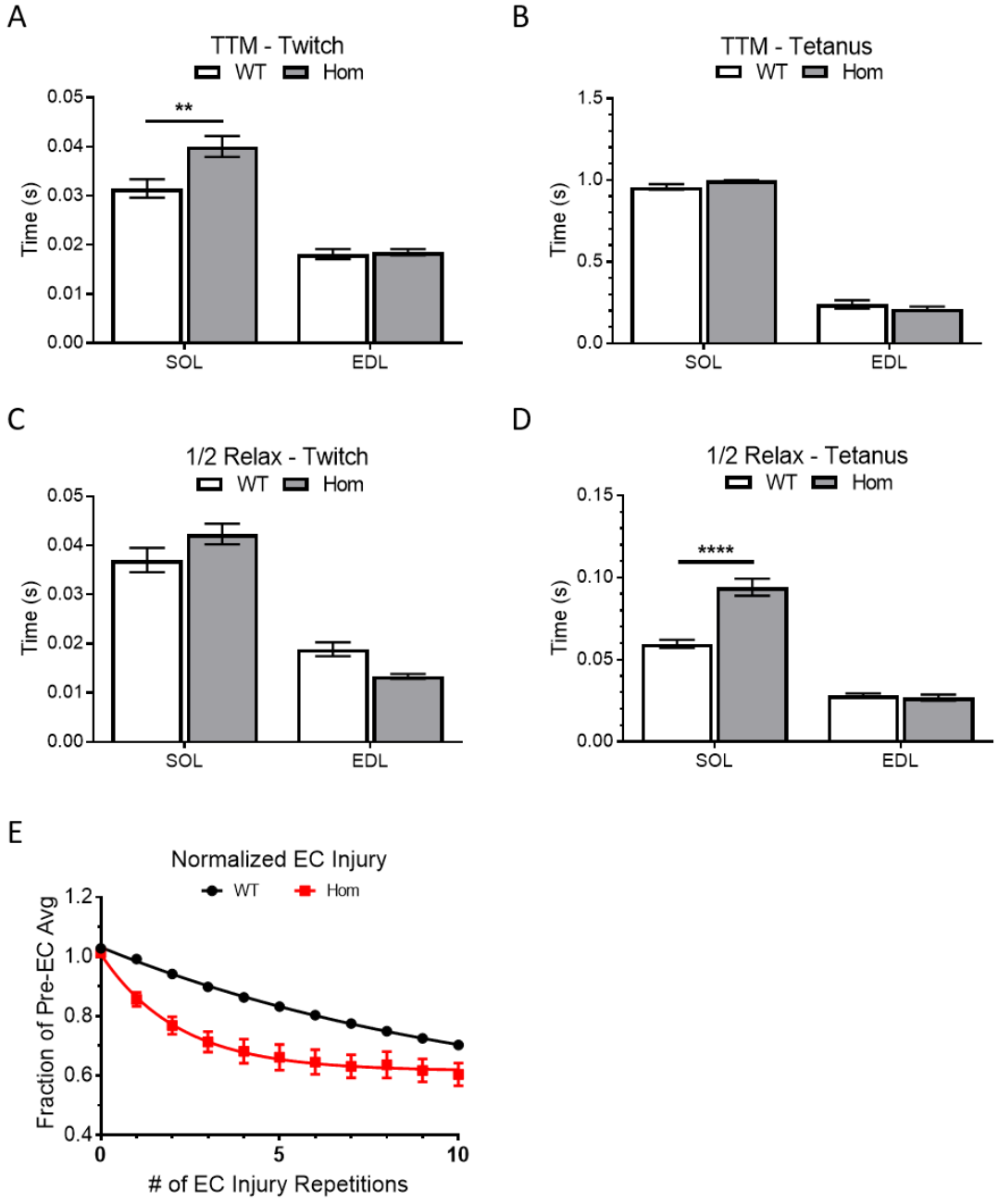

Aim 3: Study of Protein Interactions with Nebulin's C-terminus

GST pulldown experiments were run with whole muscle lysate using single-domain GST-bound constructs of the SRR and the SH3 domain as well as a two-domain construct that mirrored the endogenous C-terminus. The two-domain construct also allowed for the verification of single-domain interactions because true physiological interactions found in single-domain constructs should also interact with the two-domain construct. From two independent pulldowns of these constructs, a band appearing around 65kDa was prominent and occurred in all SRR containing domains (i.e., alone and in combination with SH3) but not when using the SH3 domain only (Figure 19). Within this band, mass spectrometry results consistently reported proteins associated with both skeletal muscle and general metabolism (Table 2). Additionally, three of these proteins have been previously reported to lead to other myopathies when disrupted: myotilin, KLHL41, and AIFM1. These proteins were chosen for further study based on their reported contributions to the sarcomeres and reported associations with myopathies.

Myotilin, a prominent regulator of Z-disk width (Salmikangas et al., 1999), was significantly overexpressed in several of the limb muscles studied. KLHL41, a nemaline myopathy-associated gene (Gupta et al., 2013), did not show significant increases in specific limb muscles, though through two-way ANOVA, there is an overall increase in protein expression. Finally, AIFM1 was found to mimic myotilin expression, with significantly higher expression found in the TC, EDL, gastrocnemius, and quadriceps. Considering this protein's role in apoptosis (Ghezzi et al., 2010), changes in this protein may also contribute to the myopathy phenotype observed.

Figure 19: GST Pulldown of Nebulin's C-terminus

Pulldown experiments to investigate binding partners of the SRR. A) Section of an 8% acrylamide gel revealing the most prominent band located within the pulldown using a GST-tagged SRR at approximately 65kDa. This band is also found in the GST construct containing both the SRR and the SH3 domain. B) Western blot examples for myopathy-related proteins found in pulldown. C) Protein expression of myotilin (n=6). TC, EDL, gastrocnemius, and quadriceps all significantly increased. Two-way ANOVA also shows significant increases in protein expression in homozygous mice compared to wild-type. D) Protein expression of KLHL41 (n=6). A global increase in homozygous tissue protein expression compared to wild-type is observed. E) Protein expression of AIFM1 (n=6). EDL, gastrocnemius, and quadriceps have significant increases. TC has a trending increase (p=0.07). Two-way ANOVA also shows significant increases in protein expression in homozygous mice compared to wild-type.

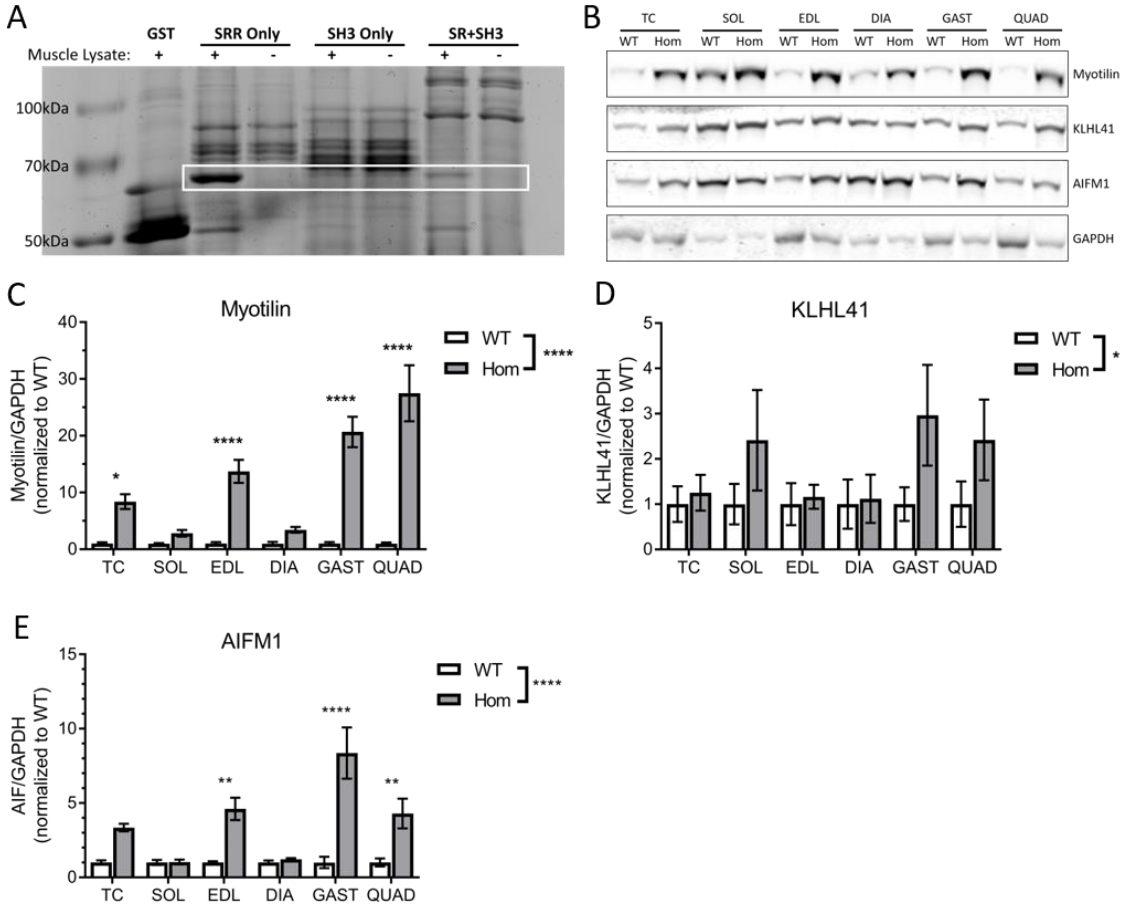

Table 2: GST Pulldown Results

Summary of proteins found within the 65kDa band of the GST-tagged SRR pulldown. Results shown were present in two separate pulldown experiments. Bolded proteins were studied via western blot.

Recurring Proteins	Associated Myopathy	Unique Peptides
Myotilin	**Myofibrillar Myopathy (Selcen & Engel, 2004)**	**7**
KLHL41	**Nemaline Myopathy (Gupta et al., 2013)**	**5**
AIFM1	**Encephalomyopathy (Ghezzi et al., 2010)**	**5**
ACADVL	Myopathy in Late-Onset VLCAD Deficiency (Ogilvie et al., 1994)	14
ATAD3	None (Mitochondrial Activity), Loss in muscles leads to myopathy phenotype (Peralta et al., 2018)	9
ARFGAP2	None (Protein Metabolism)	6
HNRNPK	None (mRNA Metabolism and Transport)	3

Aim 4: Assessing Muscle Hypertrophy Using an IGF-1 AAV

Based on a novel hypertrophy model (Takano et al., 2010), it is expected that the loss of nebulin's C-terminal domains attenuates the hypertrophy response to IGF-1 stimulus. In short, this is because nebulin's SRR is proposed to be phosphorylated by GSK-3β, preventing the interaction between the SH3 domain and the branched actin-forming protein, N-WASP. Through IGF-1 stimulation GSK-3β is inhibited, allowing for this interaction to occur and leading to myofibrillar hypertrophy. To test this mechanism, TC muscles were subjected to an intramuscular injection of an IGF-1 AAV and the effect was quantified for both the TC and the neighboring EDL after one month. One-way ANOVA, showed that IGF-1 increased TC and EDL weights in wild-type mice by ~15% (Figure 20). However, the homozygous muscles responded in a similar manner and a similar ~15% increase in weights was observed. A quantification of the individual fibers from the AAV-treated EDL found no significant differences between the wild-type and homozygous hypertrophy response in each fiber type.

Figure 20: IGF-1 AAV-Induced Hypertrophy

Intramuscular injection of IGF-1 AAV shows that the hypertrophy pathway is not inhibited by loss of the C-terminus. A) Changes observed between treated and untreated legs for both TC and EDL (n=10,7). Intramuscular injections performed on TC and AAV diffuses to the EDL. Injected TCs are significantly heavier than the PBS-injected TCs. Diffused EDLs trend to higher weights as well. C) Percent change of the leg injected with the AAV compared to the PBS-injected leg. No significant differences found in muscle weight change. D) Fiber-type specific width analysis performed using MinFeret values. Percent change between AAV-injected and sham-injected legs reported, no significant differences found in fiber hypertrophy.

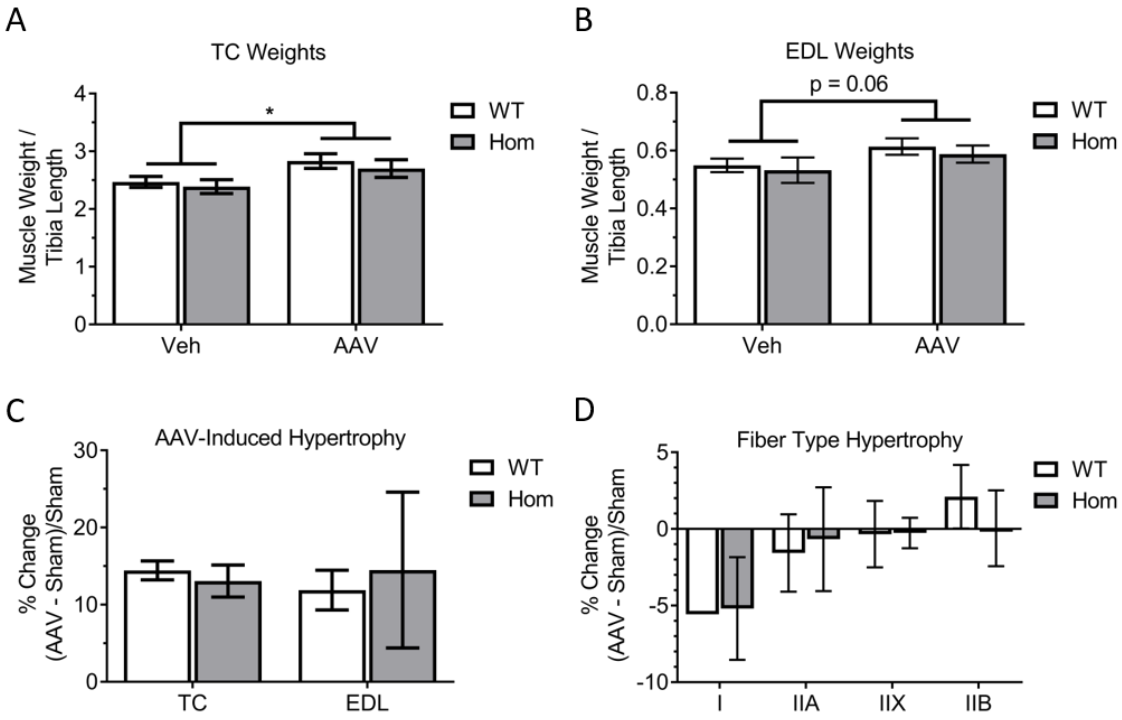

Chapter 4: Discussion

For many years, understanding of how nebulin functions in the muscle sarcomere remained relatively basic. Studies showed that it was a major contributor to nemaline myopathy (Pelin et al., 1999), but the consensus remained that the protein was primarily responsible for thin filament length regulation. It was not until full nebulin knockout mouse models were created that additional functions were discovered (Bang et al., 2006; Witt et al., 2006). With these studies came the acknowledgement that nebulin contributed to more than just thin filament lengths. Using those conventional knockout models, multiple studies elucidated nebulin's contributions to force production, calcium cycling, and sarcomere alignment (Chandra et al., 2009; Ottenheijm et al., 2008; Tonino et al., 2010). One study even attempted to increase force production in myopathic muscles by increasing cross-bridge cycling kinetics (Lee et al., 2013). However, these studies that utilized the conventional knockout model were hindered by the model's fragility and the limitation that these mice would die within two weeks of birth. Therefore, the first step to improving our understanding of how nebulin contributes to the muscle sarcomere was to develop models that better mimicked the patient condition. Through this, a better understanding of nebulin deficiency in developed sarcomeres could be established.

Simultaneously, through multiple studies on nebulin binding partners (Bang et al., 2001; Eulitz et al., 2013; Ma & Wang, 2002; Takano et al., 2010; Witt et al., 2006), it was apparent that simply knocking out the entirety of nebulin would result in many finer details of this protein's function being masked by a multitude of compensatory measures. Due to the large size of nebulin, it is reasonable to assume that at least some of the phenotypes observed in the conventional model was in part caused by compensatory changes in the sarcomere. The only domain-specific study utilizing a

nebulin truncation revealed a minimal function of the SH3 domain (limiting eccentric contraction damage) (Yamamoto et al., 2013) but nothing that related to nebulin's more established functions of thin filament length regulation, force production, or structural regulation of the Z-disks (Bang et al., 2006; Chandra et al., 2009; Li et al., 2015; Tonino et al., 2010; Witt et al., 2006). It was however proposed that the serine-rich region acted as a signaling hub or that the two domains together had a greater function on the sarcomere (Yamamoto et al., 2013). Therefore, this dissertation also examined a novel nebulin model that exhibits a more severe myopathy phenotype, compared to the SH3 knockout model, through the removal of only two C-terminal domains, the serine-rich region (SRR) and the SH3 domain. Through this truncation, the experiments showed that these C-terminal domains play a significant role in developing the structural and functional integrity of the sarcomere and loss of these domains is sufficient to invoke a nemaline myopathy phenotype.

Conditional Nebulin Knockout

Basic Phenotypes of Neb cKO Mice

This model is the first nebulin knockout model that reaches adulthood while expressing very little nebulin. While the goal was to mimic a typical nemaline myopathy, the phenotypes observed were closer to that of severe nemaline myopathy. Neb cKO mice quickly exhibit a developmental delay shortly after birth. This results in smaller mice and high mortality until around three months of age, past which mice have a higher rate of survival. This likely correlates with the importance of nebulin during development because three months is around when mice are considered fully matured and many developmental processes have slowed (Flurkey, M. Currer, & Harrison, 2007). This contrasts sharply with the conventional nebulin knockout mice, in which all die within the first two weeks of life (Bang et al., 2006; Witt et al., 2006). This suggests that nebulin assists in the development of sarcomeres around or before postnatal day zero, a function which has a severely deleterious effect on the mouse if it does not occur. This period of development has yet to be fully explored and may reveal more about nebulin's role in sarcomeric development in initial disease progression. Finally, it was noted that while all limb muscles studied eventually retained less than 3% of wild-type nebulin, not every limb muscle experienced the same rate of nebulin loss after the MCK promoter was activated. Slow muscles are more dependent on MCK expression (Tai et al., 2011) therefore experiencing greater Cre activity and a greater rate of nebulin loss. However, both slow-type muscles (soleus and diaphragm) also retain more nebulin at the three week time point (Figure 8). One explanation could be that these muscles had a higher rate of nebulin translation during embryonic development, causing the muscles to retain nebulin even as new transcripts were prevented. To verify this would require a study of nebulin protein expression at or just before birth, when the MCK promoter has not yet

become fully active (Franco, Lamers, & Moorman, 1998). Through the observations made in this model, we were able to establish that a viable nebulin knockout mouse was attainable through conditional means. This model allowed for the study of nebulin-deficient adult tissue and provided insight into phenotype progression later in development.

Fiber-Type Switching

Apart from the hypotrophy observed in several limb muscles, these muscles also had a distinctly reddish hue. From this we hypothesized that there was a deficit in metabolic processes in these muscles, changing the myoglobin content. Through SDS-PAGE analysis of MHC isoforms, it was determined that type IIB fibers were diminishing in favor of slower fiber types like type I and IIA. This shift progressed over time and affected all tissues except for the diaphragm. While studies were unable determine what was responsible for this shift, it was later noted that muscles that typically contained more type IIB fibers seemed to experience a greater degree of atrophy compared to control muscle weights (Li et al., 2015). This correlation held true in even upper limb muscles. Combined with the finding that there was a reduced tension cost in fibers (Li et al., 2015), we concluded that glycolytic fibers are more sensitive to nebulin protein loss. One explanation for this could be that glycolytic fibers have distinctly different mitochondria that function under different conditions (Mishra, Varuzhanyan, Pham, & Chan, 2015). Due to an increased ATP cost, glycolytic fibers would become extremely inefficient at contraction. This causes those fibers to be replaced by slower fiber types which are still able to contribute to force production. It should be noted that the isoform changes in the full knockout model resembled that of the nebulin truncation (discussed

later in the dissertation) and may in fact reflect a complex series of compensatory effects designed to rescue reduced force production.

Functional Changes

Intact muscle mechanics allowed for the investigation of force production in adult mice in the absence of nebulin. Here we showed that mice remain weak as adults, being unable to run to the same degree as their control counterparts. Furthermore, both the Neb cKO soleus and EDL produced significantly less normalized force, providing the reason for the reduced exercise capacity. And while additional studies performed by others during the course of this project revealed structural changes (misaligned Z-disks and protein aggregates) (Li et al., 2015), ultimately it was concluded that the primary cause for this force loss was the reduction of thin filament lengths. This coincides with published studies that had identified the drastic reduction in thin filament length as well as the loss of strict length regulation which increased the length range of thin filaments (Witt et al., 2006). This in turn would result in a reduced fraction of myosin heads being able to interact with the actin thin filaments, likely reducing the number of cross-bridges contributing to force development.

Conclusions

The development of this model was a necessity for the progression of nebulin research. Prior to this model, structural and functional studies were limited to patient samples because mouse models were still too volatile to properly study. Additionally, it was impossible to perform high throughput therapeutic studies for nemaline myopathy. By creating and characterizing the Neb cKO model, we provided a tool for future

experiments and small molecule testing. Through the characterization of this model, nebulin's role in the muscle sarcomere has been further expanded and several interesting avenues of research have been discovered. Specifically, there is now evidence that nemaline myopathy incorporates distinct metabolic changes, which may lead to the structural and functional changes normally used to characterize the disease. These nuances observed in the Neb cKO model will need to be answered to better understand both the biology of the sarcomere and the pathology of nemaline myopathy.

Nebulin Truncation and C-terminal Contributions

Viability of the Truncation Model

$Neb^{\Delta 163\text{-}165}$ mice are born at Mendelian ratios, but many homozygous mice die shortly after birth. The mice that survive exhibit a weight deficit within the first week and 87% of those remaining live into adulthood with no further complications. Surviving homozygous mice appear healthy and do not have any outward abnormalities other than a slight weight difference. Additionally, the discovery of stillborn mice only hours after birth suggests an early postnatal deficit (Figure 21). A lack of milk spots in all pups of those groups indicated that it was more likely a respiratory problem despite no drastic weight differences being observed in the diaphragm later in life (Figure 12). A possible explanation is that even slight deficits in protein expression in the diaphragm can result in contractile issues after birth, something that has been observed in infant patients (Gurgel-Giannetti et al., 2002; North et al., 1997). If this is the case, then some homozygous mice overcome this hurdle, but approximately half do not, leading to a non-Mendelian ratio when genotyped 10 days after birth. This would emphasize the role of nebulin's C-terminus in postnatal muscle development as the original conventional nebulin knockout model also exhibited severe muscle weakness at birth quickly followed by death within approximately the first week (Bang et al., 2006; Witt et al., 2006).

Figure 21: Infrequent Discovery of Stillborn Mice

Following timed breedings, there was one rare occasion where two litters were found containing stillborn pups. These pups were estimated to be only a few hours old as evidenced by the presence of an umbilical cord and a lack of milk spots. Upon genotyping the four stillborn pups found in these two litters, three were found to be homozygous while the final one was heterozygous.

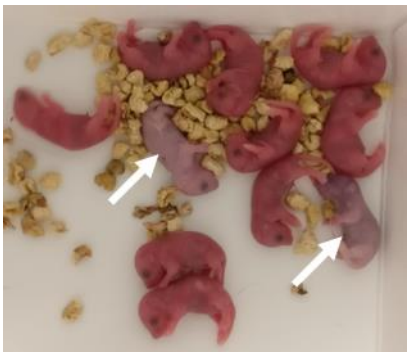

Mice expressing a truncated nebulin may be able to live longer than their conventional knockout counterparts due to their ability to produce and retain close to normal levels of nebulin. However, there does not appear to be a correlation between muscle atrophy and protein expression. For instance, while muscles like the soleus and the EDL had weights comparable to the wild-type controls, the amount of nebulin each muscle contained was unaltered in the soleus but reduced by ~40% in the EDL. Furthermore, despite varying levels of protein expression over time, the rate of muscle growth remained comparable between wild-type and homozygous mice, resulting in a consistent ratio between homozygous and wild-type weight at multiple time points (Figure 12). This suggests that there is not a direct correlation between nebulin protein expression and muscle growth. Rather, nebulin is likely to be more vital to the initial postnatal development of the sarcomeres, contributing little to muscle growth later in life. This observation is substantiated by the survival curve of the Neb cKO mice, which have an improved survivability after three months, or the primary growth phase of a mouse. The lack of worsening phenotypes also implies that structural contributions of nebulin are more important during early development. This new model shows that while the C-terminal domains of nebulin contribute to postnatal survivability, the mice surviving this initial event display a much milder myopathy phenotype than full knockout models.

Changes in MHC Fiber Content and Compensatory Effects

The truncation of nebulin resulted in all distal limb muscles experiencing a compositional shift towards slower fiber types (Figure 13). Changes in fiber type composition of sedentary mice suggest changes in the metabolic requirements and can imply a pathological origin (Zierath & Hawley, 2004). This set of experiments showed that

despite some limb muscles appearing to be unaffected by the truncation of nebulin, there was an underlying myopathy that affected all skeletal muscles.

As observed in the EDL the changes in MHC composition were not necessarily due to a loss of fast fiber types, but rather hyperplasia alongside a reduction in their cross-sectional areas. Here, the EDL, which experiences a drastic shift in fiber composition, undergoes hyperplasia, increasing the number of myofibers to maintain weight comparable to the wild-type muscle. Simultaneously, we observed hypertrophy of the slow fibers, though their inherently small population prevented them from contributing significantly to total muscle CSA. A likely scenario could be that truncation of nebulin results in muscle weakness, which in turn causes changes in protein regulation and mitochondrial biosynthesis to order to increase the size of slower fiber types (Liu, Liang, & Gan, 2015). However, because the EDL does not normally utilize many slow fibers, these changes only have a minimal effect, resulting in deficits despite attempts to compensate. Conversely, fast fibers do not tolerate changes in nebulin as well, a phenomenon documented in the conditional knockout model described earlier in this dissertation. It is possible some additional growth pathway is influencing the hyperplasia of fast fibers to maintain muscle mass and allowing the muscle to generate more force than it would have in the complete absence of nebulin. One proposed mechanism of myofibrillogenesis, specifically involving IGF-1 stimulation, is detailed later on in this discussion.

Loss of the C-terminus and Specific Nebulin Functions

In full nebulin knockout models, studies found an overall shortening of the thin filaments with an increased variation in thin filament lengths (Bang et al., 2006; Li et al., 2015; Witt et al., 2006). Filaments were found to be as short as 0.4 μm and few fibers were able to

reach the expected 1.0-1.2 µm range (Witt et al., 2006). Comparatively, such a loss in the organization of the thin filaments was not observed in the $Neb^{\Delta 163\text{-}165}$ model. Nebulin was definitively able to localize properly to the thin filaments, shown by antibodies to the N-terminus and C-terminal actin-binding modules, and the lengths observed through phalloidin staining indicated there was no difference between wild-type and homozygous mice. There were slight density changes in the A-band in the EDL when observed using electron microscopy wherein the H-zone was not well defined in homozygous EDL. This was attributed to a characteristic commonly seen in tissues with more prominent slow fiber types, namely the soleus and the heart, and seems to reflect the dramatic shift towards slower fiber types in the homozygous EDL. Overall, these findings indicate that nebulin's C-terminus is not playing a major role in thin filament length regulation.

An effect that was found is force loss, a common symptom observed in nemaline myopathy (North et al., 1997). The loss of nebulin's C-terminus appears partially responsible for the severe force loss observed in previously studied full knockout models. As observed in these experiments, both the soleus and the EDL experienced force loss at multiple time points though the loss was less apparent in the soleus (Figure 17). When considering that a deficit in protein expression may contribute to additional force loss, the soleus shows that even if a truncated nebulin is expressed to wild-type levels, there will still be a force deficit. These deficits may be related to changes observed in the Z-disk.

Though the use of electron microscopy, alterations were observed in Z-disk width, where the EDL experienced a significant increase while the soleus had a slight, but significant decrease. The differences in change could be hinting at the C-terminus's contribution to width as well. Additionally, the observation of protein aggregates in line with the Z-disks suggests that protein turnover is also partially compromised within the Z-disk, resulting in

the formation of nemaline rod bodies through a small truncation of nebulin. The truncation appears to be destabilizing the Z-disk structure, which would impair any contributions it may have to overall force production (Luther, 2009). These findings suggest that nebulin's C-terminus has a partial contribution to force generation, possibly through its interaction with other proteins that maintain the stability of the Z-disk.

Serine-Rich Region and Myopathy Phenotypes

While the SRR has been proposed to facilitate C-terminal localization of nebulin to the Z-disks (Panaviene & Moncman, 2007), it has not been studied in animal model systems. Conversely, the SH3 domain has been much more prominently featured in functional studies (Bang et al., 2001; Eulitz et al., 2013; Ma & Wang, 2002; Takano et al., 2010; Witt et al., 2006). When the SH3 domain deletion model did not reveal any myopathy phenotypes or changes in previously predicted protein interactions, the SRR became the target of our studies. A standard GST-pulldown with three different combinations of the two domains as bait was performed to elucidate this domain. Considering the results from single-domain and two-domain constructs, a prominent band observed at around 65kDa represented interactions with the removed domains. Interestingly, this band was not replicated in the SH3 domain pulldown suggesting that the interactions identified were specific to the serine-rich region alone. The proteins identified within this prominent band were found to be associated with metabolism, protein turnover, and structure, with three of the seven recurring proteins being contributors to various myopathies. These findings may suggest that the serine-rich region of nebulin plays an important role in the regulation of sarcomere structure and its loss may be a primary contributor to the development of myopathy.

Myotilin is a prominent regulator for the formation of the Z-disks, interacting with α-actinin and filamin-C to help stabilize the Z-disk (van der Ven et al., 2000). Mutations within this protein are also known to lead to myopathy (Salmikangas et al., 1999). AIFM1 on the other hand is a pro-apoptotic protein that additionally helps maintain mitochondrial bioenergetics (Hangen, Blomgren, Bénit, Kroemer, & Modjtahedi, 2010). Both myotilin and AIFM1 were differentially upregulated in the skeletal muscle studied. Specifically, both proteins appeared to be more upregulated in muscles that normally have more fast fibers. For myotilin, this may be related to changes observed at the Z-disk, particularly in the EDL (Figure 16), with widening Z-disks and protein aggregates a result of its upregulation. These findings also coincide with reports that overexpression of myotilin can worsen a myopathy phenotype, wherein mice had a more rapid onset of myofibrillar aggregation and more severe muscular degeneration (Garvey, Liu, Miller, & Hauser, 2008). AIFM1 is more associated with the bioenergetics of cells (Hangen et al., 2010) and its upregulation appears to correlate instead with the changes in fiber composition (Figure 13). That both proteins are more upregulated in fast muscles suggests muscle type-specific alterations caused by the truncation of nebulin. One possibility is that the SRR is a signaling hub that helps regulate both the Z-disk widths and sarcomere energetics. An increase in tension cost (Li et al., 2015) results in an attempt to produce more ATP, resulting in AIFM1 being upregulated. Simultaneously, myotilin becomes overexpressed as the fibers take on traits of slower fiber types, leading to both widening Z-disks and an increase of protein aggregate presence (Figure 16). Further investigation of these protein interactions may help explain why faster muscle types exhibit more severe myopathy phenotypes than slower muscle types (Li et al., 2015).

KLHL41, on the other hand, can lead to nemaline myopathy when mutated (Gupta et al., 2013). Recently, its ability to stabilize nebulin and prevent myopathy was also elucidated (Ramirez-Martinez et al., 2017). In the $Neb^{\Delta 163\text{-}165}$ model, KLHL41 was not significantly upregulated in any one muscle, though two-way ANOVA indicated that the genotype was having a significant effect on protein expression. This slight upregulation may indicate that KLHL41 does not rely wholly on the SRR for its function. Also, the previous characterization of KLHL41 utilized its interaction with nebulin's super-repeats (Ramirez-Martinez et al., 2017), suggesting that that this protein interacts with multiple regions of nebulin. A more in depth study on the interaction between KLHL41 and the SRR needs to be performed to clarify how it impacts the published function in nebulin stabilization (Ramirez-Martinez et al., 2017).

Hypertrophy and Nebulin

Based on the study of nebulin's contribution to myofibrillar hypertrophy, nebulin's SH3 domain interacts with the branched actin-forming protein N-WASP while the SRR acting as a phosphorylation site regulating this interaction (Takano et al., 2010). The $Neb^{\Delta 163\text{-}165}$ model makes it possible to critically test this proposed mechanism through the removal of those two key domains. An IGF-1 AAV was used to create a chronic overexpression of the signaling protein. This would elucidate the differences in muscle hypertrophy caused by these missing domains. However, chronic elevation of IGF-1 failed to reveal a difference between wild-type and homozygous mice. The injected TC in both genotypes underwent the same amount of hypertrophy and the neighboring EDL followed that same trend. Studies on individual fiber types also failed to reveal any significant differences in the hypertrophic response. This finding is supported by the published SH3 deletion model, where they also failed to reproduce the nebulin-N-WASP interaction

following acute IGF-1 stimulation (Yamamoto et al., 2013). Thus, nebulin's C-terminus does not appear to be a limiting factor for the proposed IGF-1 hypertrophy mechanism. This does, however, imply that nemaline myopathy patients exhibiting C-terminal truncations may still benefit from therapeutics utilizing the IGF-1 pathway. Further experiments should be done to determine why a non-linear actin forming protein like N-WASP would be localizing to the Z-disks and if there is a C-terminal independent mechanism influencing the formation of new actin filaments.

Conclusions

Nebulin's C-terminus plays a crucial role in early postnatal development of muscles. Loss of C-terminal domains induces a fast-to-slow compositional shift in muscle fibers, which in turn results in changes in Z-disk structure. This two-domain truncation affects force output, resulting in reduced forces at all time points tested. However, once those early developmental changes are set, the mouse continues to develop and the myopathy phenotypes do not worsen. The cause for these changes may in part be attributed to the lost interactions with the signaling region that is the serine-rich region. Finally, despite the myopathic changes in both sarcomere structure and function studies revealed that the IGF-1 growth pathway was still fully functional, which provides a potential therapeutic option for patients with truncated nebulin.

Final Comparisons Between Models

When considering the findings of the two models discussed in this dissertation, key differences help identify phenotypes specific to alterations in nebulin. As stated previously, a major limitation to full knockout models is the fact that nebulin participates in many functions within the sarcomere including thin filament length regulation, force production, and regulation of the Z-disks. Its loss forces the sarcomere to adapt, which may account for many of the phenotypes observed in nemaline myopathy patients. The domain-specific model attempts to mitigate some of these compensatory effects in order to better understand nebulin's function. A comparison of these two models also shows how severe myopathy may differ from a milder myopathy observed in patients.

A major point of comparison is the limb muscle weights observed in these models. The Neb cKO model has a severe atrophy occurring in most of the limb muscles and an unexpected hypertrophy occurring in the soleus. For instance, the gastrocnemius and quadriceps are nearly reduced by 80% of wild-type weights by the 6-month time point. Conversely, the soleus is increased by 50%. On the other hand, the deficit shown in the $Neb^{\Delta 163\text{-}165}$ quadriceps is milder and no hypertrophy is found in the soleus. Taking into account the differences in all muscles, it appears that the hypertrophy observed in the Neb cKO model may be resulting from overload hypertrophy, a phenomenon in which synergist muscles are unable to contribute to carrying the body's weight and, thus, healthier muscles are forced to compensate for the load (Booth & Thomason, 1991). This point is emphasized when considering the force production, which when normalized to the physiological CSA, shows that the soleus still has a significant force deficit in the Neb cKO model. It is clear that a complete loss of nebulin results in more severe atrophy, but it must be taken into account that some of the atrophy may be amplified by changes observed in different atrogenes as well (Li et al., 2015). The $Neb^{\Delta 163\text{-}165}$ model

shows instead how important the C-terminal domains are to the development a healthy sarcomere and that their loss is sufficient to produce a myopathy phenotype.

Similarities between homozygous mice of the two models in MHC composition suggest these isoform changes are caused by the loss of nebulin's C-terminus specifically. And while it was difficult to determine the mechanisms causing this isoform shift, ATPase studies in the Neb cKO model showed that fibers had an increased tension cost, which could contribute to the shift (Li et al., 2015). This hypothesis was further supported through the GST pulldown studies done on nebulin's C-terminal domains, where most of the mass spectrometry results pointed to proteins that played a role in bioenergetics. Specifically, AIFM1 appeared to be upregulated in tissues that normally would express higher type IIB content. Together, this suggests that, due to inefficient energy usage, muscles attempt to compensate by changing MHC isoforms and increasing mitochondrial content, resulting in a general shift towards slower fiber types. This hypothesis may explain how impairment of nebulin's contributions to the sarcomere leads to the changes often associated with nemaline myopathy.

Changes in sarcomere structure and function were surprisingly similar in the two models. Both models experienced force deficit and both models had prominent protein aggregates in line with the Z-disks. The difference in the magnitude of change highlights the contributions of the C-terminus compared to that of the remainder of the protein. This is an important discovery because it suggests that nebulin's C-terminus singlehandedly contributes to a significant fraction of force loss and structural change observed in the full knockout. Through electron microscopy, we were able to quantify the changes at the Z-disk and can conclude that the loss of nebulin's C-terminus destabilizes the Z-disk, causing changes in the expression of Z-disk proteins as well as preventing width regulation. This results in a loss of force that may be proportional to the force normally

contributed by the Z-disk (Luther, 2009). In this aspect, the Neb$^{\Delta 163\text{-}165}$ model shows that the C-terminus plays an important role in the regulation of the Z-disks.

The finding that loss of nebulin's C-terminus is sufficient to induce nemaline myopathy is promising for future studies into nebulin function and this disease. The results show that the C-terminus plays some major role in early postnatal development, as attributed to the postnatal deaths inferred by a skewed Mendelian ratio. However, once the muscles are fully developed, loss of nebulin's C-terminus appears to be tolerated, though it clearly continues to interfere with proper sarcomeric structure, with the retention of protein aggregates and sarcomeric disorganization in adult muscles. Studies into these domains should focus on the contributions of the C-terminus in adult tissue, for instance a timed removal of these domains in early adulthood. It will be interesting to see if this conditional removal results in a late-onset nemaline myopathy, or no changes whatsoever. Overall, there is still scientific and clinical merit in the study of nebulin's C-terminus and it should be carefully considered when undertaking functional studies of this protein.

Chapter 5: Future Directions

Contribution of Conserved Serines in the SRR to Hypertrophy

Introduction

Takano et al., 2010 investigated two conserved serines within the SRR and found that they were the targets of inhibitory phosphorylation by GSK-3β (Figure 3). By mutating those serines to aspartic acid or glutamic acid, they induced a pseudo-phosphorylated state, preventing the nebulin-N-WASP interaction from occurring. An additional phosphorylation study was performed on the $Neb^{\Delta 163\text{-}165}$ mouse model and found that the homozygous EDL had reduced growth signaling (Figure 22), which likely contributes to the reduced CSAs in fast fiber types (Figure 13). Quantification of total GSK-3β from this study reveals that the EDL is upregulating total protein expression (data not shown), which results in a decreased growth response. And while we have shown that nebulin's C-terminus is not a limiting step in hypertrophy signaling, it is by no means the only growth signaling pathway that would be affected by changes in GSK-3β activity. Thus, this study aims to specifically test the contributions of the conserved serines within the SRR to muscle growth through the use of a phospho-null mouse model. The idea behind the phospho-null SRR mouse model (NebPhospho) is that by preventing inhibitory phosphorylation of nebulin, the hypertrophy response in skeletal muscle proposed by Takano et al. 2010 can be enhanced. Once the model is sufficiently backcrossed to seven generations, studies into the hypertrophy response can be performed.

Figure 22: SRR Phosphorylation and Hypertrophy

Brief study of GSK-3β phosphorylation in $Neb^{\Delta 163\text{-}165}$ model and initial study of nebulin phospho-null SRR model (NebPhospho). A,B) S9 phosphorylation normalized to total GSK-3β in soleus and EDL. S9 phosphorylation is representative of inhibition, showing that homozygous EDL has decreased growth signaling (Jope & Johnson, 2004).

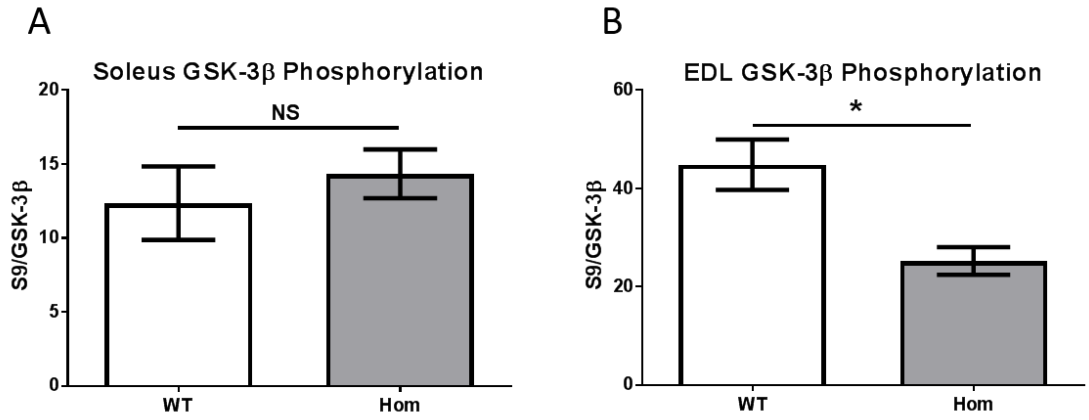

Proposed Studies

Basic characterization of this mouse model must first be done to establish baseline conditions of various limb muscles. This will involve comparisons in body weight, muscle weight, and fiber distribution. The hypothesis here is that mice with the phospho-null mutation will exhibit greater muscle growth and weights due to an inability to regulate the IGF-1 mediated growth pathway. In the most extreme case where these two serines are vitally important to the regulation of muscle growth, mice may even resemble myostatin knockout mice where muscles grow uncontrollably. However, should there be no noticeable difference, it may simply be that the proposed mechanism is one that only participates during induced hypertrophy. To determine if induced hypertrophy would cause unregulated growth, we propose to perform synergist ablations on the mice. Briefly, the entirety of the myotendinous junction of the gastrocnemius will be removed from both legs. Control mice will undergo the same surgical prep and incision, but the muscles and tendons will remain intact. Four groups will be utilized: control sham, control ablated, homozygous sham, and homozygous ablated. The expected result here is that synergist muscles undergo severe hypertrophy following the loss of the gastrocnemius (Armstrong, Marum, Tullson, & C. W. Saubert, 1979). Following this surgery, mice will be housed for two weeks before being sacrificed and their synergist muscle weights measured.

Discussion

Should experiments in the NebPhospho mice show that homozygous mice undergo greater hypertrophy than the controls, it would support the idea that the phosphorylation of these two conserved serines in the SRR regulates the hypertrophic response. This would further implicate nebulin's C-terminal domains in muscle development and

suggest that the SRR could be a target for therapeutics. And while we found the loss of the C-terminus did not restrict IGF-1 induced hypertrophy, this proposed pathway has yet to be fully examined to rule out the effects of phosphorylation of the SRR.

Upon further investigation of hypertrophic growth pathways, there arose the concern that a functional IGF-1 signaling may not be necessary for this load-induced hypertrophy (Spangenburg, Le Roith, Ward, & Bodine, 2008), suggesting that a synergist ablation procedure may not be optimal to test IGF-1 mediated hypertrophy involving nebulin's C-terminus (Takano et al., 2010). This seems to be because the hypertrophy that occurs during synergist ablation is caused primarily by an IGF-1 independent pathway that still activates Akt (PKB). However, because the downstream effectors are still activated, synergist ablation can still be used to assess the phosphorylation aspect involving nebulin's C-terminus. Concurrent to performing synergist ablations, studies also need to be done on various hypertrophy and atrophy genes. This will help elucidate the proposed mechanism involving nebulin's C-terminus. These experiments will quantify and compare expressions in key proteins (such as eIF4G, p70S6K, MuRF1, and MAFbx) in samples from both the NebPhospho model as well as the $Neb^{\Delta 163\text{-}165}$ model.

It may also be worthwhile to further investigate the role of GSK-3β in this pathway. As previously noted, S9 phosphorylation in the $Neb^{\Delta 163\text{-}165}$ model, which normally inhibits function, is reduced. Similar studies should be performed on the NebPhospho model in order to determine if there are any alterations in this pathway contributing to a hypertrophy response. For instance, if inhibitory phosphorylation of GSK-3β is decreased and yet homozygous muscles still show increased hypertrophy, it would support the role of nebulin's SRR in the hypertrophy response. Experiments could also be done where GSK-3 is specifically inhibited in both wildtype and homozygous muscles in order to compare hypertrophic response.

Finally, to fully understand the contribution of nebulin's SRR to muscle growth, additional mouse models could be utilized. One necessary mouse model would involve a phosphomimetic substitution of the two conserved serines in the SRR, replacing the conserved serines with aspartic acid or glutamic acid. Similar to the findings in Takano et al., 2010, this would theoretically prevent interactions between nebulin and N-WASP, thereby preventing hypertrophy. In this model, one might expect a lack of hypertrophic response during IGF-1 stimulation or maybe even a myopathic mouse depending on the importance of these two residues. The other, less precise, mouse model would be one where only the SRR is removed from the nebulin transcript. Studies of this model would help further clarify the necessity of nebulin's C-terminal domains to both sarcomeric development and hypertrophy.

AAV-Induced Rescue of Nemaline Myopathy Phenotype

Introduction

With the understanding that nebulin's C-terminus plays a major role in the development of nemaline myopathy, the next step is to determine if restoration of the C-terminus could ameliorate the severe myopathy phenotypes observed in the Neb cKO model. While recent studies have primarily focused on the restoration of force through enhancing contractile properties (de Winter et al., 2013; Lee et al., 2013), no study has actively attempted to replace nebulin in deficient muscles. This is primarily because nebulin is a massive protein and full-length protein expression is impossible *in vitro*. Thus, the goal is to generate a nebulin fragment that contains functionally important domains of nebulin in an attempt to improve the conditions of the sarcomeres.

Proposed Studies

In these experiments, mice will be injected at weaning age (21 days) with AAV constructs intended to help restore muscle structure and function in nebulin knockout mice. The two constructs being tested are as follows. The first is an AAV containing 1 super-repeat plus the entirety of nebulin's Z-disk domains, which includes individual actin-binding modules and the two unique C-terminal domains. The second AAV lacks the Z-disk and C-terminal domains. Each of these constructs also have a FLAG tag and an HA tag integrated into it, allowing for identification in muscle samples. The hypothesis here is that mice injected with the construct containing nebulin's C-terminus will exhibit a restoration of force and structure while those injected with only the super-repeat portion will not. The experiments will be carried out following the same protocol as the IGF-1 AAV experiments in the $Neb^{\Delta 163\text{-}165}$ model. Following a one-month incubation, muscles are to be dissected and either flash frozen or embedded in OCT for cryosectioning.

Additionally, both EDLs will be dissected for whole muscle mechanics. Stored samples can then be utilized for western blot and immunohistochemistry.

Western blot studies will assess construct expression through FLAG-tag signal in both the TC (injected target) and the EDL (offhand target). Using immunofluorescence, we will determine if the constructs are being properly localized to the Z-disks and if different fibers have differing levels of construct expression. Also, changes in fiber CSAs may also be studied using these antibodies. To perform simultaneous intact muscle mechanics on left and right EDLs, two separate setups will be used. Efforts will be made to maintain similar conditions between the two machines, including stimulation voltage and solution temperature. Individual optimal lengths (L_0) will be taken and the PCSA-normalized forces were compared. Finally, collected samples will also be embedded for immunoelectron microscopy studies. These studies will gauge thin filament lengths, as well as the size and distribution of protein aggregates (nemaline rod bodies).

Discussion

The first step is to perform the rescue experiments using the SR+Z-disk AAV. This would provide insight into whether or not restoration of nebulin's C-terminus could improve structural maintenance and allow the sarcomeres to clear out these aggregates. Once this portion of the project is completed, experiments need to be repeated with the Z-disk lacking AAV (SR-Z-Disk AAV). This provides a negative control for the effects of the other AAV. The expectation here is that treating knockout muscles with only the super-repeat domains will have a minimal effect on force production and structure. Together, these two AAVs will not only answer whether or not it is possible to rescue myopathy phenotypes when nebulin is completely absent, but also elucidate the contribution of nebulin's C-terminus in the maintenance of adult muscle.

Once structure and function have been addressed, it would be prudent to test if restoration of a small nebulin isoform has a more beneficial effect on healthier mice. One drawback of the Neb cKO model is that it still has a fairly high mortality until three months of age. By that time point, muscles are highly myopathic and the alterations in structure may already be irreversible. It also makes therapeutic experiments risky because knockout mice may randomly die during the incubation period. By utilizing a healthier model, such as the $Neb^{\Delta 163\text{-}165}$ model or even a compound heterozygous model that mimics a mild nemaline myopathy, results may be more definitive as to whether or not this AAV can have a positive therapeutic effect.

Deficient Bioenergetics in Nemaline Myopathy

It has been well established in cardiac muscle that alterations in bioenergetics can contribute to or even cause disease (reviewed in (Vakrou & Abraham, 2014)). Changes observed in contractile efficiency could easily be caused by mitochondrial dysfunction, leading to compensatory changes in structure and function as see in hypertrophic cardiomyopathy. Similarly, inefficient usage of ATP, as seen in nebulin knockout mice and nemaline myopathy patients (Li et al., 2015; Ottenheijm et al., 2010), may be a core contributor to pathology. One hypothesis is that deficient usage of ATP leads to the phenotypes observed in nemaline myopathy patients. Inefficient usage of ATP would lead to decreased muscle growth (reduced mechanical input) and an increased need for ATP production. This leads to increased mitochondria synthesis and MHC isoforms shift as a result. Improper MHC distribution would further contribute to force loss because slow fibers produce less force per unit than faster fibers (Bottinelli, Schiaffino, & Reggiani, 1991). The observation that MHC isoform distribution is relatively normal around birth (Li et al., 2015) suggests that changes are a result of deficits already present at birth, of which ATP usage in muscle contraction is a primary factor. Combined with study detailing the effects of nebulin on cross-bridge cycling (Ottenheijm et al., 2008), it is highly likely force loss is a downstream phenotype stemming from inefficient energy usage. And because a similar MHC isoform shift was observed in the $Neb^{\Delta 163\text{-}165}$ model, there is now evidence that C-terminal loss is sufficient to induce this change.

To start, it would be prudent to further characterize tension cost in different fiber types. This would require technical skills in single fiber dissections and ATPase measurements utilized in the published study of the Neb cKO model (Li et al., 2015). This would be needed to confirm that all fibers were subject to the same inefficient energy usage. This experiment is most important to perform on the $Neb^{\Delta 163\text{-}165}$ mouse model because it

would highlight the importance of nebulin's C-terminus in changes that may be leading to nemaline myopathy. Specifically, the soleus needs to be verified because it not only has normal protein expression, it also has force loss and structural changes. Simultaneously, changes in mitochondrial distribution need to be determined. This can be done through both electron microscopy as well as immunohistochemistry, staining for succinate dehydrogenase. Doing so would provide an overview for how myopathic muscles are dealing with the increased tension cost and would support that MHC isoform changes are in response to muscles attempting to compensate for inefficient ATP usage. If there is an increase in mitochondrial count or even size, this would help explain the shifts in MHC isoform and support the hypothesis that inefficient energy usage is a core cause of nemaline myopathy. Once this was determined, changes in mitochondrial function could be assessed through an array of western blot studies on each complexes of the electron transport chain. Supporting experiments could be performed by examining PGC-1α expression, which is associated with oxidative fiber development and increases during fast-to-slow fiber shifts (Chan & Arany, 2014; Lin et al., 2002).

Finally, studies should be performed to determine if there is a connection between loss of nebulin's C-terminus and sarcomere bioenergetics. As reported in the $Neb^{\Delta 163\text{-}165}$ model, there are changes in AIFM1, which could be indicative of increased mitochondrial count. Interestingly, while AIFM1 is often reported to participate in apoptosis, it also contributes to proliferation through the inhibition of PTEN oxidation, indirectly promoting the PI3K/Akt pathway (Shen et al., 2015). From a recent review of the protein, it appears that its function may differ based on its localization (Bano & Prehn, 2018), so it would be crucial to know what fraction of AIFM1 exists in the mitochondria (metabolism and growth) and what fraction is in other compartments, such as the cytosol or the nucleus

(cell death). A better understanding of this protein, and muscle mitochondria in general, would elucidate the bioenergetics component of nemaline myopathy.

References

Agrawal, P. B., Greenleaf, R. S., Tomczak, K. K., Lehtokari, V.-L., Wallgren-Pettersson, C., Wallefeld, W., . . . Beggs, A. H. (2007). Nemaline Myopathy with Minicores Caused by Mutation of the CFL2 Gene Encoding the Skeletal Muscle Actin–Binding Protein, Cofilin-2. *The American Journal of Human Genetics, 80*(1), 162-167. doi:https://doi.org/10.1086/510402

Armstrong, R. B., Marum, P., Tullson, P., & C. W. Saubert, t. (1979). Acute hypertrophic response of skeletal muscle to removal of synergists. *Journal of Applied Physiology, 46*(4), 835-842. doi:10.1152/jappl.1979.46.4.835

Bang, M.-L., Li, X., Littlefield, R., Bremner, S., Thor, A., Knowlton, K. U., . . . Chen, J. (2006). Nebulin-deficient mice exhibit shorter thin filament lengths and reduced contractile function in skeletal muscle. *The Journal of Cell Biology, 173*(6), 905-916. doi:10.1083/jcb.200603119

Bang, M.-L., Mudry, R. E., McElhinny, A. S., Trombitás, K., Geach, A. J., Yamasaki, R., . . . Labeit, S. (2001). Myopalladin, a Novel 145-Kilodalton Sarcomeric Protein with Multiple Roles in Z-Disc and I-Band Protein Assemblies. *The Journal of Cell Biology, 153*(2), 413-428. doi:10.1083/jcb.153.2.413

Bano, D., & Prehn, J. H. M. (2018). Apoptosis-Inducing Factor (AIF) in Physiology and Disease: The Tale of a Repented Natural Born Killer. *EBioMedicine, 30*, 29-37. doi:10.1016/j.ebiom.2018.03.016

Barton, E. R. (2006). Viral expression of insulin-like growth factor-I isoforms promotes different responses in skeletal muscle. *Journal of Applied Physiology, 100*(6), 1778-1784. doi:10.1152/japplphysiol.01405.2005

Booth, F. W., & Thomason, D. B. (1991). Molecular and cellular adaptation of muscle in response to exercise: perspectives of various models. *Physiological Reviews, 71*(2), 541-585. doi:10.1152/physrev.1991.71.2.541

Bottinelli, R., Schiaffino, S., & Reggiani, C. (1991). Force-velocity relations and myosin heavy chain isoform compositions of skinned fibres from rat skeletal muscle. *The Journal of Physiology, 437*, 655-672.

Burkholder, T. J., Fingado, B., Baron, S., & Lieber, R. L. (1994). Relationship between muscle fiber types and sizes and muscle architectural properties in the mouse hindlimb. *Journal of Morphology, 221*(2), 177-190. doi:doi:10.1002/jmor.1052210207

Chan, M. C., & Arany, Z. (2014). The Many roles of PGC-1α in Muscle – Recent Developments. *Metabolism: clinical and experimental, 63*(4), 441-451. doi:10.1016/j.metabol.2014.01.006

Chandra, M., Mamidi, R., Ford, S., Hidalgo, C., Witt, C., Ottenheijm, C., . . . Granzier, H. (2009). Nebulin Alters Cross-bridge Cycling Kinetics and Increases Thin Filament Activation: A NOVEL MECHANISM FOR INCREASING TENSION AND REDUCING TENSION COST. *The Journal of Biological Chemistry, 284*(45), 30889-30896. doi:10.1074/jbc.M109.049718

de Winter, J. M., Buck, D., Hidalgo, C., Jasper, J. R., Malik, F. I., Clarke, N. F., . . . Granzier, H. (2013). Troponin activator augments muscle force in nemaline myopathy patients with nebulin mutations. *Journal of Medical Genetics, 50*(6), 383-392. doi:10.1136/jmedgenet-2012-101470

Donner, K., Ollikainen, M., Ridanpää, M., Christen, H.-J., Goebel, H. H., de Visser, M., . . . Wallgren-Pettersson, C. (2002). Mutations in the β-tropomyosin (TPM2) gene – a rare cause of nemaline myopathy. *Neuromuscular Disorders, 12*(2), 151-158. doi:https://doi.org/10.1016/S0960-8966(01)00252-8

Elliott, A. (1979). Structure of molluscan thick filaments: A common origin for diverse appearances. *Journal of Molecular Biology, 132*(3), 323-340. doi:https://doi.org/10.1016/0022-2836(79)90263-8

Eulitz, S., Sauer, F., Pelissier, M.-C., Boisguerin, P., Molt, S., Schuld, J., . . . Fürst, D. O. (2013). Identification of Xin-repeat proteins as novel ligands of the SH3 domains of nebulin and nebulette and analysis of their interaction during myofibril formation and remodeling. *Molecular Biology of the Cell, 24*(20), 3215-3226. doi:10.1091/mbc.E13-04-0202

Flurkey, K., M. Currer, J., & Harrison, D. E. (2007). Chapter 20 - Mouse Models in Aging Research. In J. G. Fox, M. T. Davisson, F. W. Quimby, S. W. Barthold, C. E. Newcomer, & A. L. Smith (Eds.), *The Mouse in Biomedical Research (Second Edition)* (pp. 637-672). Burlington: Academic Press.

Franco, D., Lamers, W. H., & Moorman, A. F. M. (1998). Patterns of expression in the developing myocardium: towards a morphologically integrated transcriptional model. *Cardiovascular Research, 38*(1), 25-53. doi:10.1016/S0008-6363(97)00321-0

Garvey, S. M., Liu, Y., Miller, S. E., & Hauser, M. A. (2008). Myotilin overexpression enhances myopathology in the LGMD1A mouse model. *Muscle & Nerve, 37*(5), 663-667. doi:doi:10.1002/mus.20994

Ghezzi, D., Sevrioukova, I., Invernizzi, F., Lamperti, C., Mora, M., D'Adamo, P., . . . Zeviani, M. (2010). Severe X-Linked Mitochondrial Encephalomyopathy Associated with a Mutation in Apoptosis-Inducing Factor. *American Journal of Human Genetics, 86*(4), 639-649. doi:10.1016/j.ajhg.2010.03.002

Grove, B. K., Kurer, V., Lehner, C., Doetschman, T. C., Perriard, J. C., & Eppenberger, H. M. (1984). A new 185,000-dalton skeletal muscle protein detected by monoclonal antibodies. *The Journal of Cell Biology, 98*(2), 518-524. doi:10.1083/jcb.98.2.518

Gupta, Vandana A., Ravenscroft, G., Shaheen, R., Todd, Emily J., Swanson, Lindsay C., Shiina, M., . . . Beggs, Alan H. (2013). Identification of KLHL41 Mutations Implicates BTB-Kelch-Mediated Ubiquitination as an Alternate Pathway to Myofibrillar Disruption in Nemaline Myopathy. *American Journal of Human Genetics, 93*(6), 1108-1117. doi:10.1016/j.ajhg.2013.10.020

Gurgel-Giannetti, J., Gurgel-Giannetti, J., Bang, M.-L., Reed, U., Marie, S., Zatz, M., . . . Vainzof, M. (2002). *Lack of the C-terminal domain of nebulin in a patient with nemaline myopathy* (Vol. 25).

Hangen, E., Blomgren, K., Bénit, P., Kroemer, G., & Modjtahedi, N. (2010). Life with or without AIF. *Trends in Biochemical Sciences, 35*(5), 278-287. doi:https://doi.org/10.1016/j.tibs.2009.12.008

Huxley, H., & Hanson, J. (1954). Changes in the Cross-Striations of Muscle during Contraction and Stretch and their Structural Interpretation. *Nature, 173*, 973. doi:10.1038/173973a0

Johnston, J. J., Kelley, R. I., Crawford, T. O., Morton, D. H., Agarwala, R., Koch, T., . . . Biesecker, L. G. (2000). A Novel Nemaline Myopathy in the Amish Caused by a Mutation in Troponin T1. *The American Journal of Human Genetics, 67*(4), 814-821. doi:https://doi.org/10.1086/303089

Jope, R. S., & Johnson, G. V. W. (2004). The glamour and gloom of glycogen synthase kinase-3. *Trends in Biochemical Sciences, 29*(2), 95-102. doi:https://doi.org/10.1016/j.tibs.2003.12.004

Kazmierski, S. T., Antin, P. B., Witt, C. C., Huebner, N., McElhinny, A. S., Labeit, S., & Gregorio, C. C. (2003). The Complete Mouse Nebulin Gene Sequence and the Identification of Cardiac Nebulin. *Journal of Molecular Biology, 328*(4), 835-846. doi:https://doi.org/10.1016/S0022-2836(03)00348-6

Kruger, M., Wright, J., & Wang, K. (1991). Nebulin as a length regulator of thin filaments of vertebrate skeletal muscles: correlation of thin filament length, nebulin size, and epitope profile. *The Journal of Cell Biology, 115*(1), 97-107.

Labeit, S., Gibson, T., Lakey, A., Leonard, K., Zeviani, M., Knight, P., . . . Trinick, J. (1991). Evidence that nebulin is a protein-ruler in muscle thin filaments. *FEBS Letters, 282*(2), 313-316. doi:doi:10.1016/0014-5793(91)80503-U

Labeit, S., Kohl, C. H., Witt, C. C., Labeit, D., Jung, J., & Granzier, H. (2010). Modulation of Muscle Atrophy, Fatigue and MLC Phosphorylation by MuRF1 as Indicated by Hindlimb Suspension Studies on MuRF1-KO Mice. *Journal of Biomedicine and Biotechnology, 2010*, 693741. doi:10.1155/2010/693741

Labeit, S., & Kolmerer, B. (1995a). The complete primary structure of human nebulinand its correlation to muscle structure. *Journal of Molecular Biology, 248*(2), 308-315. doi:https://doi.org/10.1016/S0022-2836(95)80052-2

Labeit, S., & Kolmerer, B. (1995b). Titins: Giant Proteins in Charge of Muscle Ultrastructure and Elasticity. *Science, 270*(5234), 293-296. doi:10.1126/science.270.5234.293

Laing, N. G., Wilton, S. D., Akkari, P. A., Dorosz, S., Boundy, K., Kneebone, C., . . . Haan, E. (1995). A mutation in the α tropomyosin gene TPM3 associated with autosomal dominant nemaline myopathy. *Nature Genetics, 9*, 75. doi:10.1038/ng0195-75

Lee, E.-J., De Winter, J. M., Buck, D., Jasper, J. R., Malik, F. I., Labeit, S., . . . Granzier, H. (2013). Fast Skeletal Muscle Troponin Activation Increases Force of Mouse Fast Skeletal Muscle and Ameliorates Weakness Due to Nebulin-Deficiency. *PLOS ONE, 8*(2), e55861. doi:10.1371/journal.pone.0055861

Lehtokari, V. L., Kiiski, K., Sandaradura, S. A., Laporte, J., Repo, P., Frey, J. A., . . . Wallgren-Pettersson, C. (2014). Mutation Update: The Spectra of Nebulin Variants and Associated Myopathies. *Human Mutation, 35*(12), 1418-1426. doi:doi:10.1002/humu.22693

Li, F., Buck, D., De Winter, J., Kolb, J., Meng, H., Birch, C., . . . Granzier, H. L. (2015). Nebulin deficiency in adult muscle causes sarcomere defects and muscle-type-dependent changes in trophicity: novel insights in nemaline myopathy. *Human Molecular Genetics, 24*(18), 5219-5233. doi:10.1093/hmg/ddv243

Lin, J., Wu, H., Tarr, P. T., Zhang, C.-Y., Wu, Z., Boss, O., . . . Spiegelman, B. M. (2002). Transcriptional co-activator PGC-1α drives the formation of slow-twitch muscle fibres. *Nature, 418*, 797. doi:10.1038/nature00904

Liu, J., Liang, X., & Gan, Z. (2015). Transcriptional regulatory circuits controlling muscle fiber type switching. *Science China Life Sciences, 58*(4), 321-327. doi:10.1007/s11427-015-4833-4

Luther, P. K. (2009). The vertebrate muscle Z-disc: sarcomere anchor for structure and signalling. *Journal of Muscle Research and Cell Motility, 30*(5-6), 171-185. doi:10.1007/s10974-009-9189-6

Ma, K., & Wang, K. (2002). Interaction of nebulin SH3 domain with titin PEVK and myopalladin: implications for the signaling and assembly role of titin and nebulin. *FEBS Letters, 532*(3), 273-278. doi:doi:10.1016/S0014-5793(02)03655-4

Mishra, P., Varuzhanyan, G., Pham, A. H., & Chan, D. C. (2015). Mitochondrial dynamics is a distinguishing feature of skeletal muscle fiber types and regulates organellar compartmentalization. *Cell metabolism, 22*(6), 1033-1044. doi:10.1016/j.cmet.2015.09.027

North, K. N., Laing, N. G., & Wallgren-Pettersson, C. (1997). Nemaline myopathy: current concepts. The ENMC International Consortium and Nemaline Myopathy. *Journal of Medical Genetics, 34*(9), 705-713.

North, K. N., & Ryan, M. M. (2002). Nemaline Myopathy. from GeneReviews® [Internet] https://www.ncbi.nlm.nih.gov/books/NBK1288/

Nowak, K. J., Wattanasirichaigoon, D., Goebel, H. H., Wilce, M., Pelin, K., Donner, K., . . . Laing, N. G. (1999). Mutations in the skeletal muscle α-actin gene in patients with actin myopathy and nemaline myopathy. *Nature Genetics, 23*, 208. doi:10.1038/13837

Ottenheijm, C. A. C., Fong, C., Vangheluwe, P., Wuytack, F., Babu, G. J., Periasamy, M., . . . Granzier, H. (2008). Sarcoplasmic reticulum calcium uptake and speed of relaxation are depressed in nebulin-free skeletal muscle. *The FASEB Journal, 22*(8), 2912-2919. doi:10.1096/fj.07-104372

Ottenheijm, C. A. C., Hidalgo, C., Rost, K., Gotthardt, M., & Granzier, H. (2009). ALTERED CONTRACTILITY OF SKELETAL MUSCLE IN MICE DEFICIENT IN TITIN'S M-BAND REGION. *Journal of Molecular Biology, 393*(1), 10-26. doi:10.1016/j.jmb.2009.08.009

Ottenheijm, C. A. C., Hooijman, P., DeChene, E. T., Stienen, G. J., Beggs, A. H., & Granzier, H. (2010). ALTERED MYOFILAMENT FUNCTION DEPRESSES FORCE GENERATION IN PATIENTS WITH NEBULIN-BASED NEMALINE MYOPATHY (NEM2). *Journal of structural biology, 170*(2), 334-343. doi:10.1016/j.jsb.2009.11.013

Panaviene, Z., & Moncman, C. L. (2007). Linker region of nebulin family members plays an important role in targeting these molecules to cellular structures. *Cell and Tissue Research, 327*(2), 353-369. doi:10.1007/s00441-006-0305-2

Pelin, K., Hilpelä, P., Donner, K., Sewry, C., Akkari, P. A., Wilton, S. D., . . . Wallgren-Pettersson, C. (1999). Mutations in the nebulin gene associated with autosomal recessive nemaline myopathy. *Proceedings of the National Academy of Sciences, 96*(5), 2305-2310. doi:10.1073/pnas.96.5.2305

Ramirez-Martinez, A., Cenik, B. K., Bezprozvannaya, S., Chen, B., Bassel-Duby, R., Liu, N., & Olson, E. N. (2017). KLHL41 stabilizes skeletal muscle sarcomeres by nonproteolytic ubiquitination. *eLife, 6*, e26439. doi:10.7554/eLife.26439

Ravenscroft, G., Miyatake, S., Lehtokari, V.-L., Todd, Emily J., Vornanen, P., Yau, Kyle S., . . . Laing, Nigel G. (2013). Mutations in KLHL40 Are a Frequent Cause of Severe Autosomal-Recessive Nemaline Myopathy. *American Journal of Human Genetics, 93*(1), 6-18. doi:10.1016/j.ajhg.2013.05.004

Ren, R., Mayer, B., Cicchetti, P., & Baltimore, D. (1993). Identification of a ten-amino acid proline-rich SH3 binding site. *Science, 259*(5098), 1157-1161. doi:10.1126/science.8438166

Salmikangas, P., Mykkänen, O.-M., Grönholm, M., Heiska, L., Kere, J., & Carpén, O. (1999). Myotilin, a Novel Sarcomeric Protein with Two Ig-like Domains, is Encoded by a Candidate Gene for Limb-Girdle Muscular Dystrophy. *Human Molecular Genetics, 8*(7), 1329-1336. doi:10.1093/hmg/8.7.1329

Sambuughin, N., Yau, K. S., Olivé, M., Duff, R. M., Bayarsaikhan, M., Lu, S., . . . Goldfarb, L. G. (2010). Dominant Mutations in KBTBD13, a Member of the BTB/Kelch Family, Cause Nemaline Myopathy with Cores. *The American Journal of Human Genetics, 87*(6), 842-847. doi:https://doi.org/10.1016/j.ajhg.2010.10.020

Shen, S.-M., Guo, M., Xiong, Z., Yu, Y., Zhao, X.-Y., Zhang, F.-F., & Chen, G.-Q. (2015). AIF inhibits tumor metastasis by protecting PTEN from oxidation. *EMBO Reports, 16*(11), 1563-1580. doi:10.15252/embr.201540536

Shy, G. M., Engel, W. K., Somers, J. E., & Wanko, T. (1963). NEMALINE MYOPATHYA NEW CONGENITAL MYOPATHY. *Brain, 86*(4), 793-810. doi:10.1093/brain/86.4.793

Smith, L. R., & Barton, E. R. (2014). SMASH – semi-automatic muscle analysis using segmentation of histology: a MATLAB application. *Skeletal Muscle, 4*, 21. doi:10.1186/2044-5040-4-21

Spangenburg, E. E., Le Roith, D., Ward, C. W., & Bodine, S. C. (2008). A functional insulin-like growth factor receptor is not necessary for load-induced skeletal

muscle hypertrophy. *The Journal of Physiology, 586*(Pt 1), 283-291. doi:10.1113/jphysiol.2007.141507

Suetsugu, S., Miki, H., Yamaguchi, H., Obinata, T., & Takenawa, T. (2001). Enhancement of branching efficiency by the actin filament-binding activity of N-WASP/WAVE2. *Journal of Cell Science, 114*(24), 4533-4542.

Tai, P. W. L., Fisher-Aylor, K. I., Himeda, C. L., Smith, C. L., MacKenzie, A. P., Helterline, D. L., . . . Hauschka, S. D. (2011). Differentiation and fiber type-specific activity of a muscle creatine kinase intronic enhancer. *Skeletal Muscle, 1*, 25-25. doi:10.1186/2044-5040-1-25

Takano, K., Watanabe-Takano, H., Suetsugu, S., Kurita, S., Tsujita, K., Kimura, S., . . . Endo, T. (2010). Nebulin and N-WASP Cooperate to Cause IGF-1–Induced Sarcomeric Actin Filament Formation. *Science, 330*, 1536-1540.

Talmadge, R. J., & Roy, R. R. (1993). Electrophoretic separation of rat skeletal muscle myosin heavy-chain isoforms. *Journal of Applied Physiology, 75*(5), 2337-2340. doi:10.1152/jappl.1993.75.5.2337

Tonino, P., Pappas, C. T., Hudson, B. D., Labeit, S., Gregorio, C. C., & Granzier, H. (2010). Reduced myofibrillar connectivity and increased Z-disk width in nebulin-deficient skeletal muscle. *Journal of Cell Science, 123*, 384-391.

Vakrou, S., & Abraham, M. R. (2014). Hypertrophic cardiomyopathy: a heart in need of an energy bar? *Frontiers in Physiology, 5*, 309. doi:10.3389/fphys.2014.00309

van der Ven, P. F. M., Wiesner, S., Salmikangas, P., Auerbach, D., Himmel, M., Kempa, S., . . . Fürst, D. O. (2000). Indications for a Novel Muscular Dystrophy Pathway. *γ-Filamin, the Muscle-Specific Filamin Isoform, Interacts with Myotilin, 151*(2), 235-248. doi:10.1083/jcb.151.2.235

Wallgren-Pettersson, C., Kääriäinen, H., Rapola, J., Salmi, T., Jääskeläinen, J., & Donner, M. (1990). Genetics of congenital nemaline myopathy: a study of 10 families. *Journal of Medical Genetics, 27*(8), 480-487.

Warren, C. M., Krzesinski, P. R., & Greaser, M. L. (2003). Vertical agarose gel electrophoresis and electroblotting of high-molecular-weight proteins. *ELECTROPHORESIS, 24*(11), 1695-1702. doi:doi:10.1002/elps.200305392

Witt, C. C., Burkart, C., Labeit, D., McNabb, M., Wu, Y., Granzier, H., & Labeit, S. (2006). Nebulin regulates thin filament length, contractility, and Z-disk structure in vivo. *The EMBO Journal, 25*(16), 3843-3855. doi:10.1038/sj.emboj.7601242

Yamamoto, D. L., Vitiello, C., Zhang, J., Gokhin, D. S., Castaldi, A., Coulis, G., . . . Bang, M.-L. (2013). The nebulin SH3 domain is dispensable for normal skeletal muscle structure but is required for effective active load bearing in mouse. *Journal of Cell Science, 126*(23), 5477-5489. doi:10.1242/jcs.137026

Young, P., Ehler, E., & Gautel, M. (2001). Obscurin, a giant sarcomeric Rho guanine nucleotide exchange factor protein involved in sarcomere assembly. *The Journal of Cell Biology, 154*(1), 123-136. doi:10.1083/jcb.200102110

Yuen, M., Sandaradura, S. A., Dowling, J. J., Kostyukova, A. S., Moroz, N., Quinlan, K. G., . . . Clarke, N. F. (2015). Leiomodin-3 dysfunction results in thin filament disorganization and nemaline myopathy. *The Journal of Clinical Investigation, 125*(1), 456-457. doi:10.1172/JCI80057

Zierath, J. R., & Hawley, J. A. (2004). Skeletal Muscle Fiber Type: Influence on Contractile and Metabolic Properties. *PLoS Biology, 2*(10), e348. doi:10.1371/journal.pbio.0020348